AGU PUBLICATIONS

JGR

Journal of Geophysical Research: Earth Surface

RESEARCH ARTICLE
10.1002/2014JF003279

Key Points:
- Vertical acceleration plays a fundamental role in granular mass flow dynamics
- Nonhydrostatic effects are introduced into a general depth-averaged model
- The theory allows for modeling flows over 3-D terrain mathematically

Correspondence to:
O. Castro-Orgaz,
oscarcastro@ias.csic.es;
ag2caoro@uco.es

Citation:
Castro-Orgaz, O., K. Hutter, J. V. Giraldez, and W. H. Hager (2015), Nonhydrostatic granular flow over 3-D terrain: New Boussinesq-type gravity waves?, *J. Geophys. Res. Earth Surf.*, *120*, 1–28, doi:10.1002/2014JF003279.

Received 14 JUL 2014
Accepted 27 NOV 2014
Accepted article online 3 DEC 2014
Published online 13 JAN 2015

Nonhydrostatic granular flow over 3-D terrain: New Boussinesq-type gravity waves?

Oscar Castro-Orgaz[1], Kolumban Hutter[2], Juan V. Giraldez[3], and Willi H. Hager[4]

[1]Hydraulic Engineering Area, University of Cordoba, Cordoba, Spain, [2]TU Darmstadt, Darmstadt, Germany, [3]Department of Agronomy, IAS-CSIC and University of Córdoba, Cordoba, Spain, [4]VAW, ETH Zurich, Zurich, Switzerland

Abstract Understanding granular mass flow is a basic step in the prediction and control of natural or man-made disasters related to avalanches on the Earth. Savage and Hutter (1989) pioneered the mathematical modeling of these geophysical flows introducing Saint-Venant-type mass and momentum depth-averaged hydrostatic equations using the continuum mechanics approach. However, Denlinger and Iverson (2004) found that vertical accelerations in granular mass flows are of the same order as the gravity acceleration, requiring the consideration of nonhydrostatic modeling of granular mass flows. Although free surface water flow simulations based on nonhydrostatic depth-averaged models are commonly used since the works of Boussinesq (1872, 1877), they have not yet been applied to the modeling of debris flow. *Can granular mass flow be described by Boussinesq-type gravity waves*? This is a fundamental question to which an answer is required, given the potential to expand the successful Boussinesq-type water theory to granular flow over 3-D terrain. This issue is explored in this work by generalizing the basic Boussinesq-type theory used in civil and coastal engineering for more than a century to an arbitrary granular mass flow using the continuum mechanics approach. Using simple test cases, it is demonstrated that the above question can be answered in the affirmative way, thereby opening a new framework for the physical and mathematical modeling of granular mass flow in geophysics, whereby the effect of vertical motion is mathematically included without the need of ad hoc assumptions.

1. Introduction

Many natural or man-made disasters are caused by mass movement all over the Earth's surface. Mass movement types range from rock avalanches, for which the fluid pore pressure is negligible, to saturated debris flow, where the fluid enhances mass displacement [*Iverson*, 1997; *Iverson and Denlinger*, 2001]. Physical mathematical models for mass movement provide a solid foundation to investigate the behavior of geophysical flows [*Iverson*, 2014]. These models are based on mass and momentum conservation equations using the continuum mechanics approach. Mass and momentum conservation equations have been in use to model water flows for more than a century, since Saint-Venant presented his classic depth-averaged water flow equations. This mathematical tool is relatively new in debris flow modeling, however. The simplest model for rapid flow of debris masses was introduced by *Savage and Hutter* [1989, 1991], who developed depth-averaged mass and momentum conservation equations for a one-phase grain case. Their theory (now called the Savage-Hutter (SH) equations) set up a new perspective into the dynamics of granular materials; it was elaborated on and generalized by *Hutter and Koch* [1991], *Hutter et al*. [1993], *Iverson et al*. [1997], *Gray et al*. [1999], *Denlinger and Iverson* [2001], *Iverson and Denlinger* [2001], *Iverson and Vallance* [2001], *Pudasaini and Hutter* [2003], *Pudasaini et al*. [2003, 2005a, 2005b, 2008], *Wang et al*. [2004]; *Chiou et al*. [2005], *Hutter* [2005], *Hutter et al*. [2005], *Luca et al*. [2009a, 2009b, 2009c, 2012], *Hutter and Luca* [2012], and *Wieland et al*. [1999]. *Hutter* [1996] and *Pudasaini and Hutter* [2007] summarized the state of the art and further scrutinized and interpreted alternative formulations, e.g., by *McDougall and Hungr* [2003, 2004, 2005]. Formulations for a gravity-driven viscous fluid model in curvilinear coordinates following the basal topography were introduced by *Bouchut and Westdickenberg* [2004] with follow-up publications on SH-type formulations by *Luca et al*. [2009a, 2009b] and *Kuo et al*. [2009]. These descriptions were applied to the Tsaoling landslide [*Kuo et al*., 2009], the Shiaolin landslide [*Kuo et al*., 2010], and the Hsiaolin landslide [*Kuo et al*., 2011], all in Taiwan. Fluidized granular masses, common in nature, are often influenced by the fluid pore pressure [*Iverson*, 1997, 2005, 2014; *Savage and Iverson*, 2003; *Pudasaini et al*., 2005b]. *Iverson* [1997] presented the mixture mass and momentum equations for binary solid-fluid mixtures but simplified this concept later by identifying the constituent material velocities and reducing the momentum balances to a single balance of momentum for

the mixture as a whole; this led to an explicit account of the pore pressure as a significant dynamic agent but ignored the solid-fluid interaction force [*Iverson and Denlinger*, 2001]. The analogous approach was also taken by *Pudasaini et al*. [2005b] within a curvilinear coordinate setting. An early mixture concept for rapid debris flows was suggested by *Iverson* [1997]. It was, however, employed in a rapid shear flow context with higher generality, i.e., without imposing the assumption of vanishing relative slip of the constituents as done by *Iverson and Denlinger* [2001]. Such more general mixture settings have been described, among others, e.g., by *Pelanti et al*. [2008], *Pitman and Le*, 2005, *Pailha and Pouliquen* [2009], *Pudasaini* [2011], and *Luca et al*. [2009b]. Applications of two-layer mixture formulations are proposed by *Luca et al*. [2009c, 2012] and by *Hutter and Luca* [2012].

These formulations demonstrated the considerable advantage of the mixture formulation over the single constituent concept, as only they allow proper parameterizations of erosion and deposition processes and mass flow of the solid and fluid constituents across interior interfaces. Moreover, it is only in the context of mixture formulations that the constituent interaction forces are accounted for. Current mixture flow models for flow over three-dimensional (3-D) terrain are based on depth-averaged mass and momentum conservation equations to gain computational efficiency. Their stress tensor is defined using a Coulomb-like proportionality between shear and normal stresses [*Bagnold*, 1954; *Hungr and Morgenstern*, 1984; *Savage and Hutter*, 1989; *Iverson and Denlinger*, 2001; *Hunt et al*., 2002]. *Denlinger and Iverson* [2001] developed a depth-averaged model on a curvilinear reference system following the basal topography, as introduced by *Hutter and Savage* [1988] and *Savage and Hutter* [1989, 1991] and adopted to complex surfaces by *Gray et al*. [1999] and *Wieland et al*. [1999]. The model was a generalization to 3-D terrain and fluidized masses of the SH model (1989 and 1991). The basal curvilinear reference system corresponds to that introduced by *Dressler* [1978] to analyze water waves. The transformation of the mass and momentum equations to basal-fitted coordinates enhances the latter equations by including centripetal acceleration, which implies a nonhydrostatic pressure normal to the terrain surface. *Hutter and Savage* [1988], *Gray et al*. [1999], *Iverson and Denlinger* [2001], *Mangeney-Castelnau et al*. [2003], and *Hutter et al*. [2005] presented solutions similar to those of Saint-Venant in this reference system, some neglecting centripetal accelerations and assuming isotropic normal stresses. The basal curvilinear coordinates for the deduction of depth-averaged conservation equations of mass and momentum involve the determination of curvatures over highly irregular and rapidly changing terrain, a challenging task. This "centripetal normal stress" was added to the otherwise hydrostatic pressure parametrization. *Denlinger and Iverson* [2001] incorporated a reduced contribution of the acceleration component that is essentially perpendicular to the principal flow direction, which also occurs in gravity flow over nearly plane topography, for which Cartesian reference frames isolate this contribution.

A crucial aspect of flow over natural terrain is that the vertical velocity component is nonzero and of magnitude comparable to the hydrostatic pressure [*Iverson*, 2005; *Andreotti et al*., 2013; *Iverson*, 2014]. The only model considering such flow in a Cartesian framework appears to be the *Denlinger and Iverson* [2004] description of dry avalanches of granular materials. They presented an approximate method by introducing a mean value of the vertical acceleration in the momentum equations, estimated from a mean vertical velocity derived from kinematic boundary conditions at the free and basal surfaces. This acceleration was then coupled with the gravity acceleration to enhance the system of equations, assuming a linear distribution for the stresses in the vertical direction. *Iverson* [2014] stated that simplifying vertical velocity components causes a loss of accuracy in the momentum estimation of the mass flow. He stressed that efforts to correct the effect of the neglected or approximated momentum are only at the start in debris flow modeling, despite the long-time tradition in water flow modeling. Additionally, *Andreotti et al*. [2013] have indicated that depth-averaged models need to include vertical acceleration effects, given their fundamental role in mass flow over natural terrain. The recent remarks of these authors on the importance of depth-averaged models and the inclusion of vertical acceleration effects in the governing equations motivated the present research.

The field of water waves is rich in the use of depth-averaged models, in which the hydrostatic equation is enhanced by vertical acceleration terms. In the earlier works of *Boussinesq* [1872, 1877] this effect was accounted for into a depth-averaged model, but Serre [*Serre*, 1953; *Castro-Orgaz and Hager*, 2011] proposed a rigorous depth-averaged Boussinesq-type model for practical applications to both steady and unsteady water flow problems. This model was also developed by *Benjamin and Lighthill* [1954] following a different theoretical treatment based on a third-order expansion of the stream function. Application of Boussinesq-type equations to civil engineering was successful for the accurate description of flow over weirs, undular jumps,

sand waves, Favre waves, dam breaks, overfalls, and slope breaks [*Fawer*, 1937; *Iwasa*, 1955, 1956; *Mandrup-Andersen*, 1975, 1978; *Marchi*, 1963, 1992, 1993; *Matthew*, 1963, 1991; *Engelund and Hansen*, 1966; *Basco*, 1983; *Hager*, 1983; *Hager and Hutter*, 1984a, 1984b; *Montes*, 1986; *Soares-Frazão and Zech*, 2002; *Mohapatra and Chaudhry*, 2004; *Bose and Dey*, 2007, 2009; *Chaudhry*, 2008; *Castro-Orgaz and Hager*, 2009]. *Castro-Orgaz et al*. [2012, 2013] demonstrated that Boussinesq-type enhanced equations also describe free surface groundwater flow.

The water wave equations were further developed by *Peregrine* [1967], who obtained depth-integrated inviscid Boussinesq equations in two horizontal dimensions presenting thereby the first numerical solution for undular bore propagation. He initiated the use of Boussinesq-type equations in coastal engineering applications. This work was followed by further improvements of the analysis of the dispersive wave characteristics of the Boussinesq system, developing accurate and robust numerical schemes and including real flow features such as wave breaking, vorticity effects, and turbulence [*Mei*, 1983; *Carmo et al*., 1993; *Nwogu*, 1993; *Chen and Liu*, 1995; *Wei et al*., 1995; *Wei and Kirby*, 1995; *Madsen et al*., 1997; *Madsen and Schäffer*, 1998; *Stansby and Zhou*, 1998; *Chen et al*., 1999; *Kennedy et al*., 2000; *Lynett et al*., 2002; *Stansby*, 2003; *Chen et al*., 2003; *Erduran et al*., 2005; *Musumeci et al*., 2005; *Lynett*, 2006; *Chen*, 2006; *Soares-Frazão and Guinot*, 2008; *Mignot and Cienfuegos*, 2008; *Kim et al*., 2009; *Kim and Lynett*, 2011]. Nowadays, the governing equations and numerical techniques are in a stage of development involving a large variety of water wave phenomena [*Kim et al*., 2009; *Kim and Lynett*, 2011]. The dispersive effects caused by the vertical velocity flow component pose a problem in the treatment of depth-averaged models [*Denlinger and Iverson*, 2004]. Their model appears to be the *sole Boussinesq-type model* available for *debris flow*, a fact revealed in this work. *Denlinger and Iverson* [2004] presented the full numerical solution over 3-D terrain, but the basic features of the governing equations induced by dispersive terms were not revealed. The purpose of this work is to investigate whether nonhydrostatic granular mass flow can or should be described by Boussinesq-type gravity wave models. The dispersive treatment associated with the enhanced gravity approach is thereby assessed by generalizing the basic Boussinesq-type water wave model to debris flows.

Practically, all granular gravity-driven flow models are lowest order approximations of shallow flows, in which horizontal length scales [L] are substantially larger than vertical length scales [H]. Nondimensionalizations of the mass and momentum balance equations, based on this anisotropic scaling, then show for basically horizontal flow that the vertical acceleration terms are small of order $O(\varepsilon)$ in the aspect ratio, $\varepsilon = [H]/[L]$, so that the vertical force balance is usually expressed as a hydrostatic pressure balance. If the nondimensionalization of the governing equations is isotropic, $[L] = [H]$, the analogous scale analysis shows that the vertical acceleration term is $O(1)$ (i.e., comparable to the gravity term). In this case the full vertical momentum equation must be preserved. The Boussinesq-type model is based on this isotropic scaling. It accounts for smaller horizontal length scales, in fact, of the order of vertical length scales. This recognition is well known in hydraulic applications but has been used in granular rapid flows only by *Denlinger and Iverson* [2004]; for details see Appendix A. In a general curvilinear coordinate setting of gravity-driven geophysical flows three types of accelerations may arise that affect the internal stress distribution of free surface flows. The *first* is the acceleration due to the real forces acting on the bed. The bed-normal component of this acceleration is what makes the key effect of the Boussinesq-type model. The *second*, actually not a real acceleration, manifests itself as an enhanced pressure due to the Christoffel symbols of the curvilinear coordinate setting and is often simply referred to as centripetal acceleration. This contribution is accounted for in many granular avalanche models. The *third* are the Coriolis and centripetal accelerations due to the fact that the Earth fixed frame is not inertial. This contribution to the acceleration has never been looked at in the gravity-driven rapid flow problems. This allows for defining the focus of this work: the pure Boussinesq-type extension of the classical shallow flow description of granular avalanches. This entails using a horizontal-vertical Cartesian coordinate setting, for which only the vertical acceleration due to the vertical motion arises. More complex systems, for which two or even three of the above mentioned acceleration effects interact, are not considered herein. This description will have a significant effect on the bed-normal (true) acceleration.

The present work comprises three main parts: First, the vertically integrated equations of the continuum mechanical balance laws of mass and momentum are presented as evolution equations for the velocity field and stress tensor. After suitable approximate representations for the stress tensor, the emerging equations are applied to turbulent water flow, rock avalanches, or debris flows. Second, a scale analysis of the governing equations is introduced and Boussinesq-type equations are obtained from the vertically integrated

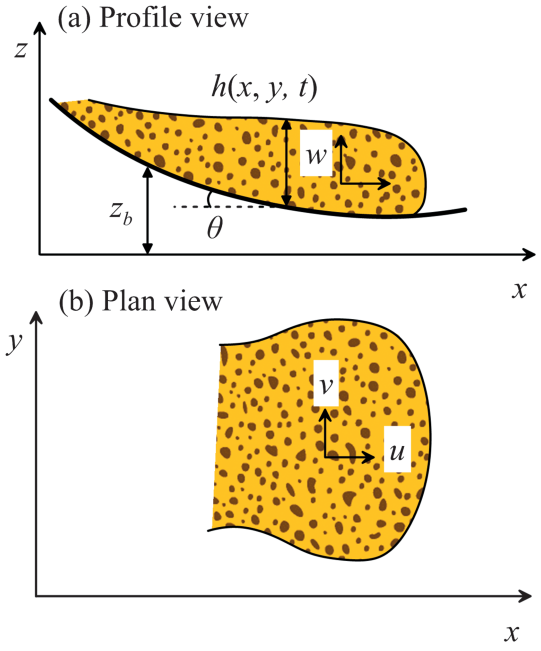

Figure 1. Definition sketch of granular mass flow over 3-D terrain.

equations. In the limit, as the shallowness parameter approaches zero, the vertically integrated equations reduce to the Saint-Venant depth-averaged equations. The new Boussinesq-type system for granular media is fully nonlinear and dispersive. Accordingly, the system of equations is closed for numerical solution once a stress tensor is prescribed for the mixture material. Third, dispersive effects are evaluated using simplified analytical solutions obtained from the general system of the depth-averaged equations. While the exact analytical solutions of simplified forms of the governing equations do not necessarily represent real cases, they provide insights in specific model aspects, as the treatment of dispersive effects. For this purpose the analytical solutions of the solitary wave and the free fall of dry granular mass flow are developed. Further, a numerical solution of flow over a hump is used to show the differences between the free material surface and the basal piezometric stress line. The full unsteady flow solution of the system of equations over 3-D terrain is beyond the scope of this work. Details of suitable numerical techniques to solve dispersive systems are provided so that the simplified analytical solutions presented apply to test cases for developing new numerical schemes. For a mixture of a number of constituents, say a solid-fluid debris flow, the balance of mass for the mixture velocity is often defined as solenoidal, and we will follow this custom here as well, but explain its restrictions in Appendix B.

2. Vertically Integrated Equations in Continuum Mechanics

2.1. Basic Conservation Laws in a Continuum Medium

Consider the flow of a granular mass of density ρ moving across a 3-D terrain (Figure 1). In a horizontal-vertical Cartesian system of reference (x, y, z) the terrain elevation is described by the function $z_b(x, y, t)$. The motion of a fluidized granular mass is described within the framework of continuum mechanics with mass and momentum conservation equations for the mixture of solids and fluid [*Savage and Hutter*, 1989; *Iverson*, 1997; *Andreotti et al.*, 2013]. The mass conservation equation states

$$\frac{\partial u}{\partial x}+\frac{\partial v}{\partial y}+\frac{\partial w}{\partial z}=0. \tag{1}$$

A vector field, whose divergence vanishes is called solenoidal, and it is known in single constituent bodies that a sufficient condition for this to hold is that the medium has constant density [e.g., *Hutter and Jőhnk*, 2004]. One says that the medium is *density preserving*. Mass balance then shows that the medium is also volume preserving. More popular is to say that the medium is incompressible. Conditions for statement (1) are explained in Appendix B.

The dynamic statement is Newton's Second Law, according to which the time rate of change of momentum equals the sum of the applied forces, given here by the stress divergence plus the gravity force, in Cartesian coordinates by

$$\frac{\partial u}{\partial t}+u\frac{\partial u}{\partial x}+v\frac{\partial u}{\partial y}+w\frac{\partial u}{\partial z}=-\frac{1}{\rho}\left(\frac{\partial \tau_{xx}}{\partial x}+\frac{\partial \tau_{xz}}{\partial z}+\frac{\partial \tau_{xy}}{\partial y}\right), \tag{2}$$

$$\frac{\partial v}{\partial t}+u\frac{\partial v}{\partial x}+v\frac{\partial v}{\partial y}+w\frac{\partial v}{\partial z}=-\frac{1}{\rho}\left(\frac{\partial \tau_{yy}}{\partial y}+\frac{\partial \tau_{yx}}{\partial x}+\frac{\partial \tau_{yz}}{\partial z}\right), \tag{3}$$

$$\frac{\partial w}{\partial t}+u\frac{\partial w}{\partial x}+v\frac{\partial w}{\partial y}+w\frac{\partial w}{\partial z}=-\frac{1}{\rho}\left(\frac{\partial \tau_{zz}}{\partial z}+\frac{\partial \tau_{zx}}{\partial x}+\frac{\partial \tau_{zy}}{\partial y}\right)-g. \tag{4}$$

The stress tensor τ_{ij}, $i,j = (x,y,z)$ is here introduced as a pressure tensor (the negative of the stress tensor in the usual notation, to conform with the notation used in the environmental contexts [e.g., *Iverson*, 1997, 2005; *Andreotti et al*., 2013]). Thus, pressures are positive normal stresses unlike in the standard notation. Equations (1)–(4) define mass and momentum conservations for single constituent bodies like water and will also be applied for a dry or fluidized granular mass, the latter in the restricted sense defined above.

Equations (1)–(4) relate the kinematic fields (u, v, w) to an arbitrary stress tensor **T**. If solids are neglected, and time averaging is performed, then **T** would describe the stress tensor of the Reynolds-Averaged Navier-Stokes (RANS) equations [*Rodi*, 1980] used to model turbulent water flows. With the sign convention used here, this means that the Reynolds stress is given by $\mathbf{T} = +\overline{\vec{u} \otimes \vec{u}}$, where $\otimes$ is the dyadic product and the overbar indicates Reynolds statistical averaging. Further, if the fluid is absent and the stress tensor is defined based on the Mohr-Coulomb model, the equations describe the motion of dry granular flow [e.g., *Savage and Hutter*, 1989; *Iverson*, 1997, 2005; *Andreotti et al*., 2013].

The full 3-D unsteady numerical solution of equations (1)–(4) is not an easy task, in particular if the constitutive relations are complex and the stress tensor **T** is accurately defined for modeling purposes [*Steffler and Jin*, 1993]. Computational effort is extremely high for large natural areas involving dense computational meshes. An approach to reduce computational efforts is to vertically integrate equations (1)–(4) to obtain vertically averaged variables as functions of only (x, y, t). Examples in hydraulic engineering are *Yen* [1973], *Steffler and Jin* [1993], *Liggett* [1994], *Vreugdenhil* [1994], *Khan and Steffler* [1996a, 1996b], and *Jain* [2001], and in rapid gravity-driven mass flows the scene has been set by *Hutter and Savage* [1988], *Savage and Hutter* [1989, 1991], and *Iverson* [1997, 2005]; it was applied in the context of laboratory avalanches by *Gray et al*. [1999], *Wieland et al*. [1999], and *Tai et al*. [2012]. For a review see, e.g., *Pudasaini and Hutter* [2007]. Thus, equations (1)–(4) provide a general starting point to produce a family of depth-averaged models within the context of continuum mechanics, valid either for water, solid particles, or—in the mentioned restricted sense—mixture flows. The current developments are particular cases for clear-water or debris flow problems.

The mathematical formulation for the derivation of depth-integrated dynamical equations in topography following coordinates was laid down by *Bouchut and Westdickenberg* [2004] for the gravity-driven flow of an ideal fluid. This procedure was followed by *Luca et al*. [2009a, 2009b] and others for debris flows. The approach in all these works is that two surface-parallel coordinates are introduced; the third coordinate is then optimally selected to be perpendicular to these, i.e., normal to the topographic surface. This defines the velocity components to be parallel and orthogonal to the basal surface (in the sense implied by the associated metric) and the depth of the flowing mass to be measured perpendicular to the basal surface. In this paper depth integration will be performed with reference to a Cartesian coordinate system; however, Boussinesq-type equations can also be derived using curvilinear coordinates.

2.2. Depth-Integrated Continuity Equation

Let the Cartesian coordinates be horizontal (x, y) and vertical (z), against gravity. Then the process consists in vertically integrating the governing equations at an arbitrary point (x, y) from z_b to z_s, where subscripts b and s, respectively, refer to the basal and free surfaces. Equation (1) then becomes

$$\int_{z_b}^{z_s} \left(\frac{\partial u}{\partial x} + \frac{\partial v}{\partial y} + \frac{\partial w}{\partial z} \right) \mathrm{d}\varsigma = 0, \tag{5}$$

where ς is the dummy variable for vertical integration. Using Leibniz's rule [*Yen*, 1973; *Hutter and Jőhnk*, 2004] equation (5) is converted to

$$\frac{\partial}{\partial x} \int_{z_b}^{z_s} u \mathrm{d}\varsigma - u_s \frac{\partial z_s}{\partial x} + u_b \frac{\partial z_b}{\partial x} + \frac{\partial}{\partial y} \int_{z_b}^{z_s} v \mathrm{d}\varsigma - v_s \frac{\partial z_s}{\partial y} + v_b \frac{\partial z_b}{\partial y} + w_s - w_b = 0. \tag{6}$$

As to the kinematic boundary conditions, the movement of the material free surface is described by

$$\frac{\partial z_s}{\partial t} + u_s \frac{\partial z_s}{\partial x} + v_s \frac{\partial z_s}{\partial y} - w_s = 0. \tag{7}$$

Similarly, the kinematic equation at the material basal surface takes the form

$$\frac{\partial z_b}{\partial t} + u_b \frac{\partial z_b}{\partial x} + v_b \frac{\partial z_b}{\partial y} - w_b = 0. \tag{8}$$

Inserting equations (7) and (8) into equation (6) produces

$$\frac{\partial h}{\partial t} + \frac{\partial Q_x}{\partial x} + \frac{\partial Q_y}{\partial y} = 0, \quad Q_x = \int_{z_b}^{z_s} u \mathrm{d}\varsigma, \quad Q_y = \int_{z_b}^{z_s} v \mathrm{d}\varsigma, \tag{9}$$

since $h = h(x,y,t) = z_s(x,y,t) - z_b(x,y,t)$ (Figure 1). Equation (9) states the general depth-integrated mass (or here volume) conservation subjected to a density-preserving body and material free and basal surfaces. The integrals in equation (9) are the fluxes Q_x and Q_y in the (x, y) directions.

2.3. Depth-Integrated Momentum Equations in Horizontal Plane

Integrating equation (2) over depth yields

$$\int_{z_b}^{z_s} \left(\frac{\partial u}{\partial t} + u \frac{\partial u}{\partial x} + v \frac{\partial u}{\partial y} + w \frac{\partial u}{\partial z} \right) \mathrm{d}\varsigma = \int_{z_b}^{z_s} -\frac{1}{\rho} \left(\frac{\partial \tau_{xx}}{\partial x} + \frac{\partial \tau_{xz}}{\partial z} + \frac{\partial \tau_{xy}}{\partial y} \right) \mathrm{d}\varsigma. \tag{10}$$

The acceleration term of the left-hand side of equation (10) may be rewritten as

$$\frac{\partial u}{\partial t} + u \frac{\partial u}{\partial x} + v \frac{\partial u}{\partial y} + w \frac{\partial u}{\partial z} = \frac{\partial u}{\partial t} + \frac{1}{2} \frac{\partial (u^2)}{\partial x} + \frac{\partial (uv)}{\partial y} + \frac{\partial (uw)}{\partial z} - u \left(\frac{\partial w}{\partial z} + \frac{\partial v}{\partial y} \right) \tag{11}$$

and with equation (1)

$$\frac{\partial u}{\partial t} + u \frac{\partial u}{\partial x} + v \frac{\partial u}{\partial y} + w \frac{\partial u}{\partial z} = \frac{\partial u}{\partial t} + \frac{\partial (u^2)}{\partial x} + \frac{\partial (uv)}{\partial y} + \frac{\partial (uw)}{\partial z}. \tag{12}$$

Inserting equation (12) into equation (10), applying the Leibniz rule, and using equations (7) and (8), the depth-integrated momentum equation in the x direction takes the form

$$\frac{\partial}{\partial t} \int_{z_b}^{z_s} u \mathrm{d}\varsigma + \frac{\partial}{\partial x} \int_{z_b}^{z_s} u^2 \mathrm{d}\varsigma + \frac{\partial}{\partial y} \int_{z_b}^{z_s} uv \mathrm{d}\varsigma = -\frac{1}{\rho} \left[\frac{\partial}{\partial x} \int_{z_b}^{z_s} \tau_{xx} \mathrm{d}\varsigma + \frac{\partial}{\partial y} \int_{z_b}^{z_s} \tau_{xy} \mathrm{d}\varsigma + (\tau_{xx})_b \frac{\partial z_b}{\partial x} + (\tau_{xy})_b \frac{\partial z_b}{\partial y} - (\tau_{xz})_b \right], \tag{13}$$

in which all stresses at the free surface have been assumed to vanish. Likewise, the depth-integrated momentum equation in the y direction is written as

$$\frac{\partial}{\partial t} \int_{z_b}^{z_s} v \mathrm{d}\varsigma + \frac{\partial}{\partial y} \int_{z_b}^{z_s} v^2 \mathrm{d}\varsigma + \frac{\partial}{\partial x} \int_{z_b}^{z_s} uv \mathrm{d}\varsigma = -\frac{1}{\rho} \left[\frac{\partial}{\partial y} \int_{z_b}^{z_s} \tau_{yy} \mathrm{d}\varsigma + \frac{\partial}{\partial x} \int_{z_b}^{z_s} \tau_{xy} \mathrm{d}\varsigma + (\tau_{yy})_b \frac{\partial z_b}{\partial y} + (\tau_{xy})_b \frac{\partial z_b}{\partial x} - (\tau_{yz})_b \right]. \tag{14}$$

The set of equations (13) and (14) describes flows with reference to the (x, y) plane. The particular case of 1-D flow in the x direction was presented by *Steffler and Jin* [1993]. Equations (13) and (14) allow for several approximations to the kinematic field (u, v, w) and parameterizations of the stress tensor $\mathbf{T}$ to produce a family of depth-averaged equations.

2.4. Integrated Momentum Equation in the *z* Direction

The integration of the vertical momentum equation is similar to the deduction of system (13) and (14). However, here equation (4) is integrated between a generic elevation z and the free surface to obtain the vertical distribution of the stress τ_{zz}, rather than the bulk vertical momentum balance to find the basal vertical stress, as in *Steffler and Jin* [1993] or *Denlinger and Iverson* [2004]. We start with the integral relation

$$\int_{z}^{z_s} \left(\frac{\partial w}{\partial t} + \frac{\partial w^2}{\partial z} + \frac{\partial (wu)}{\partial x} + \frac{\partial (wv)}{\partial y} \right) \mathrm{d}\varsigma = \int_{z}^{z_s} -\frac{1}{\rho} \left(\frac{\partial \tau_{zz}}{\partial z} + \frac{\partial \tau_{zx}}{\partial x} + \frac{\partial \tau_{zy}}{\partial y} + \rho g \right) \mathrm{d}\varsigma. \tag{15}$$

Using Leibniz' rule in equation (15) produces a vertically integrated equation with terms related to u_s, v_s, and w_s (Appendix C). These are eliminated with the aid of the free surface kinematic condition (equation (7)), resulting, with $\eta = z - z_b$ as the elevation above the local basal surface, in (Appendix C)

$$\tau_{zz}(z) = \rho g(h-\eta) - \rho w^2 + \rho \frac{\partial}{\partial t}\int_z^{z_s} w \mathrm{d}\varsigma + \rho \frac{\partial}{\partial x}\int_z^{z_s} wu \mathrm{d}\varsigma + \rho \frac{\partial}{\partial y}\int_z^{z_s} wv \mathrm{d}\varsigma + \int_z^{z_s}\left(\frac{\partial \tau_{xy}}{\partial y} + \frac{\partial \tau_{zx}}{\partial x}\right)\mathrm{d}\varsigma. \quad (16)$$

Note that ρ is taken as a constant in equations (15) and (16). This equation describes the general distribution of τ_{zz} in the z direction as a function of the vertical velocity w and the indicated stresses (last term on the right-hand side). The equation is general, allowing for a systematic development of the depth-averaged equations. Note that at the free surface the stress from equation (16) is zero, not $\tau_{zz}(z_s) = -\rho {w_s}^2$, given that one cannot simply set $z = z_s$ at the lower limit of the integrals. One must evaluate first the integrals, afterward the differentiation in front of the integral signs must be done, and only then it is possible to set $z = z_s$ in the resulting function (Appendix C). It still remains to find the general form of the profile $w(z)$. This was not presented by *Denlinger and Iverson* [2004] or *Iverson* [2005] for debris flow, whereas it is done in water wave modeling [e.g., *Nwogu*, 1993; *Kim et al.*, 2009]. It consists of integrating equation (1) between z_b and an arbitrary elevation z by using Leibniz' rule and imposing the basal kinematic condition, equation (8). The result for a rigid basal surface ($\partial z_b/\partial t = 0$) (Appendix C) takes the form

$$w(z) = -\left[\frac{\partial}{\partial x}\int_{z_b}^{z} u \mathrm{d}\varsigma + \frac{\partial}{\partial y}\int_{z_b}^{z} v \mathrm{d}\varsigma\right]. \quad (17)$$

It reveals that once any functional representations for u and v are introduced, w is determined by a simple mass (volume) conservation balance. This avoids the use of an independent function of w, given that it is linked to u and v. Equation (17) inserted into equation (16) mathematically eliminates the dependence of τ_{zz} on w.

3. Shallow Flow Approximation and Depth-Averaged Equations

If the thickness $h(x, y, t)$ of the mixture mass is smaller than the characteristic length L in the (x, y) plane (e.g., $\varepsilon = H/L << 1$, so the terrain is not steep, Appendix A), a scaling analysis reveals that, with the exception of a basal boundary layer, the velocity components u and v remain approximately constant across h, equal to their depth-averaged values U and V [*Savage and Hutter*, 1989; *Iverson*, 2005]. Therefore,

$$u(x, y, z, t) \approx U(x, y, t) = \frac{1}{h}\int_{z_b}^{z_s} u \mathrm{d}\varsigma, \quad (18)$$

$$v(x, y, z, t) \approx V(x, y, t) = \frac{1}{h}\int_{z_b}^{z_s} v \mathrm{d}\varsigma. \quad (19)$$

With this approximation a slip velocity is accepted at the bed level $z = z_b$. The depth-averaged approximation for u and v also applies if h is of the order of L, that is, $\varepsilon = O(1)$ and the terrain is steep (Appendix A), given the small contribution on the momentum equations of the differential advection originating from the nonuniformity of u and v with z (Appendix A) [*Denlinger and Iverson*, 2004]. Note that equation (18) implies that $\bar{u}^2 - (\bar{u})^2 = 0$ that is exact only if $u(z)$ is not a function of z [*Hutter et al.*, 2005]. Inserting equations (18) and (19) into equations (13) and (14) results in

$$\frac{\partial}{\partial t}(Uh) + \frac{\partial}{\partial x}\left(U^2 h\right) + \frac{\partial}{\partial y}(UV) = -\frac{1}{\rho}\left[\frac{\partial}{\partial x}\int_{z_b}^{z_s} \tau_{xx}\mathrm{d}\varsigma + \frac{\partial}{\partial y}\int_{z_b}^{z_s} \tau_{xy}\mathrm{d}\varsigma + (\tau_{xx})_b \frac{\partial z_b}{\partial x} + (\tau_{xy})_b \frac{\partial z_b}{\partial y} - (\tau_{xz})_b\right], \quad (20)$$

$$\frac{\partial}{\partial t}(Vh) + \frac{\partial}{\partial y}\left(V^2 h\right) + \frac{\partial}{\partial x}(VU) = -\frac{1}{\rho}\left[\frac{\partial}{\partial y}\int_{z_b}^{z_s} \tau_{yy}\mathrm{d}\varsigma + \frac{\partial}{\partial x}\int_{z_b}^{z_s} \tau_{xy}\mathrm{d}\varsigma + (\tau_{yy})_b \frac{\partial z_b}{\partial y} + (\tau_{xy})_b \frac{\partial z_b}{\partial x} - (\tau_{yz})_b\right]. \quad (21)$$

Moreover, the assumption of depth-independent horizontal velocity components automatically yields for the vertical velocity profile, from equation (17),

$$w = -\left[\frac{\partial}{\partial x}[U(z - z_b)] + \frac{\partial}{\partial y}[V(z - z_b)]\right]. \tag{22}$$

The vertical stress (pressure) is then, from equation (16),

$$\tau_{zz} = \rho g(h - \eta) - \rho w^2 + \rho \frac{\partial}{\partial t}\int_z^{z_s} w \mathrm{d}\varsigma + \rho \frac{\partial}{\partial x}\left[U\int_z^{z_s} w \mathrm{d}\varsigma\right] + \rho \frac{\partial}{\partial y}\left[V\int_z^{z_s} w \mathrm{d}\varsigma\right] + \int_z^{z_s}\left(\frac{\partial \tau_{xy}}{\partial y} + \frac{\partial \tau_{zx}}{\partial x}\right)\mathrm{d}\varsigma. \tag{23}$$

Note that using equations (18) and (19) both u and v have no z dependence. Thus, they can be taken out of the integral symbol in equation (16), as done in equation (23). The mass conservation equation is simply, from equation (9),

$$\frac{\partial h}{\partial t} + \frac{\partial (Uh)}{\partial x} + \frac{\partial (Vh)}{\partial y} = 0. \tag{24}$$

The depth-averaged model is given by equations (20)–(24), where the functions (u, v, w) are approximated by the functions U and V. Nothing specific is yet assumed about the stress tensor $\mathbf{T}$ so that the system of equations applies to solids, fluids, and—in the restricted sense mentioned above—mixtures. Equations (20), (21), and (24) are expressed in general conservative form as

$$\frac{\partial \mathbf{U}}{\partial t} + \frac{\partial \mathbf{F}}{\partial x} + \frac{\partial \mathbf{G}}{\partial y} = \mathbf{S}, \tag{25}$$

with

$$\mathbf{U} = \begin{pmatrix} h \\ Uh \\ Vh \end{pmatrix}, \quad \mathbf{F} = \begin{pmatrix} Uh \\ U^2 h + \frac{1}{\rho}\int_{z_b}^{z_s} \tau_{xx}\mathrm{d}\varsigma \\ UVh + \frac{1}{\rho}\int_{z_b}^{z_s} \tau_{xy}\mathrm{d}\varsigma \end{pmatrix}, \quad \mathbf{G} = \begin{pmatrix} Vh \\ VUh + \frac{1}{\rho}\int_{z_b}^{z_s} \tau_{xy}\mathrm{d}\varsigma \\ V^2 h + \frac{1}{\rho}\int_{z_b}^{z_s} \tau_{yy}\mathrm{d}\varsigma \end{pmatrix},$$
$$\mathbf{S} = -\frac{1}{\rho}\begin{pmatrix} 0 \\ (\tau_{xx})_b \frac{\partial z_b}{\partial x} + (\tau_{xy})_b \frac{\partial z_b}{\partial y} - (\tau_{xz})_b \\ (\tau_{yy})_b \frac{\partial z_b}{\partial y} + (\tau_{xy})_b \frac{\partial z_b}{\partial x} - (\tau_{yz})_b \end{pmatrix}. \tag{26}$$

The vector of dependent variables is $\mathbf{U}$, the vector of fluxes in the x direction is $\mathbf{F}$, and that in the y direction is $\mathbf{G}$, and $\mathbf{S}$ is the source term vector. Equations (22) and (23) can also be transformed to a 2-D vector notation [*Peregrine*, 1967; *Kim et al*., 2009]. Let the auxiliary variable be

$$I = \int_z^{z_s} w(x, y, z)\mathrm{d}\varsigma, \tag{27}$$

and let the depth-averaged velocity vector be

$$\mathbf{u} = \begin{pmatrix} U \\ V \end{pmatrix}. \tag{28}$$

The vertical velocity, from equation (22), may then be rewritten as

$$w = -\nabla \cdot [\mathbf{u}(z - z_b)], \tag{29}$$

in which ∇ is the 2-D nabla operator defined by

$$\nabla = \left(\frac{\partial}{\partial x}, \frac{\partial}{\partial y}\right). \tag{30}$$

Inserting equation (29) into equation (27) leads, after integration, to

$$I = -\nabla \cdot \left[\mathbf{u}\frac{(h^2-\eta^2)}{2}\right] + h[\mathbf{u} \cdot \nabla(h+z_b)]. \tag{31}$$

Equation (23) is rewritten by neglecting stress contributions (last integral of right-hand side)

$$\tau_{zz} = \rho g(h-\eta) + \rho\frac{\partial I}{\partial t} + \rho\nabla \cdot (I\mathbf{u}) - \rho w^2. \tag{32}$$

Equations (29) and (32) are the core for modeling dispersion effects in depth-averaged models; they complete the development of *Iverson* [2005].

4. Simplified Forms of Boussinesq Extended Flow Equations

In what follows, we present both hydraulic and avalanche-type examples. All, however, are restricted to using a horizontal/vertical Cartesian coordinate setting.

4.1. Hydrostatic RANS Model for River Flow

River flows are usually modeled using a Reynolds-Averaged Navier-Stokes (RANS) depth-averaged model. Stresses are then made up of viscous and turbulent contributions. If the vertical velocity is neglected, the flux vectors reduce to [*Rodi*, 1980; *Molls and Chaudhry*, 1995]

$$\mathbf{F} = \begin{pmatrix} Uh \\ U^2h + \dfrac{gh^2}{2} + \dfrac{1}{\rho}hT_{xx} \\ UVh + \dfrac{1}{\rho}hT_{xy} \end{pmatrix}, \quad \mathbf{G} = \begin{pmatrix} Vh \\ VUh + \dfrac{1}{\rho}hT_{xy} \\ V^2h + \dfrac{gh^2}{2} + \dfrac{1}{\rho}hT_{yy} \end{pmatrix}. \tag{33}$$

In these expressions the hydrostatic pressure term has been substituted, and the laminar viscous stress contributions are generally ignored. In that case, T_{xx}, T_{yy}, and T_{xy} are the depth-averaged turbulent stresses. These can be determined by coupling an auxiliary system for turbulence, e.g., the depth-averaged k-ε model, or simply by using a constant eddy viscosity [*Molls and Chaudhry*, 1995]. If turbulent stresses are neglected, the system reduces to the classical 2-D Saint-Venant equations.

4.2. Inviscid Boussinesq-Type Equations for Water Waves on a Horizontal Bottom

Consider the inviscid water wave propagation in a horizontal channel ($z_b = 0$) [*Peregrine*, 1967], for which $\tau_{xx} = \tau_{zz} = p$, which is the water pressure. In this case equation (16) (or (23) or (32)) becomes

$$p(z) = \rho g(h-\eta) - \rho w^2 + \rho\frac{\partial}{\partial t}\int_z^{z_s} w\,\mathrm{d}\varsigma + \rho\frac{\partial}{\partial x}\int_z^{z_s} wu\,\mathrm{d}\varsigma + \rho\frac{\partial}{\partial y}\int_z^{z_s} wv\,\mathrm{d}\varsigma, \tag{34}$$

in which the stress term has been ignored. This is the general equation developed by *Nwogu* [1993] for water waves. Consider the depth-averaged approach for 1-D flow, for which equations (29) and (31) reduce to

$$w = -\eta\frac{\partial U}{\partial x}, \quad I = -\frac{\partial U}{\partial x}\frac{(h^2-\eta^2)}{2}. \tag{35}$$

Inserting these into equation (34) yields a parabolic pressure distribution p consisting of a hydrostatic term plus a quadratic dynamic correction including derivatives U_{xx}, $U_x{}^2$, and U_{xt} as

$$\frac{p}{\rho} = g(h-\eta) + \left(-U_{xt} - UU_{xx} + U_x^2\right)\frac{(h^2-\eta^2)}{2}. \tag{36}$$

The subscripts indicate partial differentiations with respect to the indicated variables, i.e., $U_{xt} = \partial^2 U/\partial x\partial t$, $U_{xx} = \partial^2 U/\partial x^2$, and $U_x = \partial U/\partial x$. Equation (25) then simplifies to

$$\frac{\partial \mathbf{U}}{\partial t} + \frac{\partial \mathbf{F}}{\partial x} = \mathbf{0}, \quad \mathbf{U} = \begin{pmatrix} h \\ Uh \end{pmatrix}, \quad \mathbf{F} = \begin{pmatrix} Uh \\ M \end{pmatrix}, \quad M = U^2h + \frac{1}{\rho}\int_{z_b}^{z_s} p\,\mathrm{d}\varsigma. \tag{37}$$

M is referred to as the momentum function or flow momentum in the free surface hydraulics literature [*Montes*, 1998; *Jain*, 2001]. For this case one has

$$M = \underbrace{g\frac{h^2}{2} + U^2 h}_{\text{Saint-Venant term}} + \underbrace{\left(-U_{xt} - UU_{xx} + U_x^2\right)\frac{h^3}{3}}_{\text{Dispersive term}}. \tag{38}$$

Note that the subscripts in the dispersion terms indicate differentiation. Thus, M gives rise to higher-order equations of flow. The momentum function is composed of a Saint-Venant (hydrostatic) leading order term plus a dispersive correction. Equation (38) was originally derived by *Serre* [1953] and is extensively used in civil engineering applications [*Basco*, 1983; *Soares-Frazão and Zech*, 2002; *Mohapatra and Chaudhry*, 2004; *Chaudhry*, 2008].

4.3. Hydrostatic 1-D Dry Granular Flow Model

Consider 1-D dry granular flow with a hydrostatic pressure, for which the relation between the horizontal and vertical stresses is expressed by the earth pressure coefficient K as [*Savage and Hutter*, 1989; *Andreotti et al.*, 2013]

$$\begin{aligned} &\tau_{xx} = K\tau_{zz} = K\rho g(h-\eta), \quad \text{where} \\ &K = K_{act}, \quad \text{if} \quad \partial U/\partial x > 0, \quad K = K_{\text{pas}}, \quad \text{if} \quad \partial U/\partial x < 0. \end{aligned} \tag{39}$$

The streamwise momentum equation in the Cartesian system of reference adopted here agrees with the SH approach and is, from equation (25),

$$\frac{\partial}{\partial t}(Uh) + \frac{\partial}{\partial x}\left(U^2 h + gK\frac{h^2}{2}\right) = -gh\frac{\partial z_b}{\partial x} + \frac{(\tau_{zx})_b}{\rho}. \tag{40}$$

For a Mohr-Coulomb yield criterion with angle of internal friction ϕ_{int} and a Coulomb sliding law with basal friction angle ϕ_{bed} [see *Pudasaini and Hutter*, 2007, pp. 117–121]

$$(\tau_{zx})_b = -g\,\text{sgn}(U)h\tan\phi_{\text{bed}}, \quad K_{\text{pas/act}} = 2\sec^2\phi_{\text{int}}\left\{1 \pm \left(1 - \cos^2\phi_{\text{int}}\sec^2\phi_{\text{bed}}\right)^{1/2}\right\} - 1. \tag{41}$$

It follows that the dynamical system, equations (25) and (26) takes here the form

$$\frac{\partial \mathbf{U}}{\partial t} + \frac{\partial \mathbf{F}}{\partial x} = \mathbf{S}, \tag{42}$$

with

$$\mathbf{U} = \begin{pmatrix} h \\ Uh \end{pmatrix}, \quad \mathbf{F} = \begin{pmatrix} Uh \\ g\left(U^2 h + \frac{1}{2}Kh^2\right) \end{pmatrix}, \quad \mathbf{S} = \begin{pmatrix} 0 \\ -gh\frac{\partial z_b}{\partial x} - g\,\text{sgn}(U)h\tan\phi_{\text{bed}} \end{pmatrix}, \tag{43}$$

where K is given by equation (41).

4.4. Nonhydrostatic Dry Granular Flow Model With Enhanced Gravity

Denlinger and Iverson [2004] found that the stresses generated by granular avalanches over irregular terrain are nonhydrostatic, stating the equation of vertical pressure at the basal level as

$$(\tau_{zz})_b = \rho g h + \rho\left(\frac{\partial(\overline{w}h)}{\partial t} + \frac{\partial(\overline{w}Uh)}{\partial x} + \frac{\partial(\overline{w}Vh)}{\partial y}\right) = \rho g^{'} h. \tag{44}$$

The vertical velocity is described by the depth-averaged value

$$\overline{w}(x,y,t) = \frac{1}{h}\int_{z_b}^{z_s} w\,\mathrm{d}\varsigma. \tag{45}$$

In equation (44) g' is the enhanced gravity, including a mean vertical acceleration $\mathrm{D}\overline{w}/\mathrm{D}t$ as

$$g^{'} = g + \frac{D\overline{w}}{Dt} = g + \frac{\partial \overline{w}}{\partial t} + U\frac{\partial \overline{w}}{\partial x} + V\frac{\partial \overline{w}}{\partial y}. \tag{46}$$

As to the depth-averaged velocity, *Denlinger and Iverson* [2004] used the mean value

$$\overline{w} = \frac{1}{2}(w_s + w_b). \tag{47}$$

Here w_s and w_b are determined from equations (7) and (8), respectively. Equation (47) permits evaluation of $(\tau_{zz})_b$ from equation (44). *Denlinger and Iverson* [2004] further assumed that $\tau_{zz}(z)$ is linearly distributed as

$$\tau_{zz}(z) = \rho g'(h - \eta(z)), \tag{48}$$

the simplest continuous connection between $(\tau_{zz})_b$ and $(\tau_{zz})_s = 0$. They found that the magnitude of $\mathrm{D}\overline{w}/\mathrm{D}t$ was high in granular avalanche flows, with $(\mathrm{D}\overline{w}/\mathrm{D}t)/g$ ranging from -0.9 to $+0.6$. This suggests that the vertical acceleration is of the same order as the gravity term, implying its relevance in avalanche dynamics [*Andreotti et al*., 2013].

Given that the sole model considering this effect is the *Denlinger and Iverson* [2004] model, the physical simplifications underlying the enhanced gravity part of their model must be fully analyzed and can, indeed, be corroborated. For this purpose, from the general equation (23) at the basal level, and neglecting the stress integral we write first

$$(\tau_{zz})_b = \rho g h - \rho w_b^2 + \rho \left[\frac{\partial}{\partial t} \int_z^{z_s} w \mathrm{d}\varsigma + \frac{\partial}{\partial x} \left[U \int_z^{z_s} w \mathrm{d}\varsigma \right] + \frac{\partial}{\partial y} \left[V \int_z^{z_s} w \mathrm{d}\varsigma \right] \right]_{z=z_b}. \tag{49}$$

With the use of equation (45) this is identical to equation (44) (Appendix C). If the vertical mean value of w is computed using the general equation (29), then equation (47) results. Therefore, the basal pressure result of *Denlinger and Iverson* [2004] is an exact depth-averaged value. Second, $\tau_{zz}(z)$ as given by equation (48) is assumed to be linearly distributed, whereas a parabolic distribution results from equation (32). *Denlinger and Iverson's* [2004] approximation to the vertical stress profile introduces some error in the momentum flux computation, despite the exact basal vertical stress value. The effect of the approximation on the nonhydrostatic component in equation (44) is difficult to estimate for fully unsteady computations over 3-D terrain. However, simplified solutions may reveal an order of magnitude of this correction.

To gain some physical insight, consider 1-D *steady* dry granular flow over a horizontal plane. The momentum flux in the x direction is then

$$M = U^2 h + \frac{1}{\rho} K \int_{z_b}^{z_s} \tau_{zz} \mathrm{d}\varsigma, \tag{50}$$

or with the simple linear z dependence of equation (48)

$$M = U^2 h + K g' \frac{h^2}{2}. \tag{51}$$

In this case, according to equations (47) and (7) and since $w_b = 0$, g' reduces to

$$g' = g + \frac{U}{2} \frac{\partial w_s}{\partial x} = g + \frac{U}{2} \frac{\partial}{\partial x} \left(U \frac{\partial h}{\partial x} \right). \tag{52}$$

Consequently, since $q = Uh$ is constant in steady state, U can be replaced by q/h,

$$M = U^2 h + K \left\{ g + \frac{U}{2} (U h_x)_x \right\} \frac{h^2}{2} = U^2 h + K \left\{ g + \frac{U}{2} (U_x h_x + U h_{xx}) \right\} \frac{h^2}{2}, \tag{53}$$

and noting that $U_x = -(q/h^2) h_x$

$$M = U^2 h + K \left\{ g + \frac{U}{2} \left(-\frac{q}{h^2} h_x^2 + \frac{q}{h} h_{xx} \right) \right\} \frac{h^2}{2} = U^2 h + K \left\{ g + \frac{U^2}{2} \left(-\frac{h_x^2}{h} + h_{xx} \right) \right\} \frac{h^2}{2}, \tag{54}$$

which yields

$$M = K g \frac{h^2}{2} + \frac{q^2}{h} \left(1 + K \frac{h h_{xx} - h_x^2}{4} \right). \tag{55}$$

As above, the subscripts x denote differentiation with respect to the variable x.

For comparative purposes the present general depth-averaged model is simplified to the same conditions of dry granular 1-D steady flow. Using equations (29), (31), and (32) for 1-D, steady flow over a horizontal bed in the x direction the vertical stress distribution $\tau_{zz}(z)$ can be found. Inserting this distribution into equation (50) and performing the corresponding integral results in

$$M = Kg\frac{h^2}{2} + \frac{q^2}{h}\left(1 + K\frac{hh_{xx} - h_x^2}{3}\right). \tag{56}$$

This is a generalization for a dry granular material of the water wave equation developed by *Serre* [1953], *Benjamin and Lighthill* [1954], or *Iwasa* [1956] to study cnoidal waves and bores. Note that the water wave formulation is regained from equation (56) simply by setting $K = 1$, as deduced by *Hager and Hutter* [1984a, 1984b] using streamline coordinates. A comparison between equations (55) and (56) reveals that Denlinger and Iverson's approach introduces a factor $(\frac{1}{4})$ into the nonhydrostatic terms as compared with the exact factor $(\frac{1}{3})$ originating from the full analytical model. The effect of this factor must be investigated considering the family of equations given by

$$M = Kg\frac{h^2}{2} + \frac{q^2}{h}\left(1 + K\frac{hh_{xx} - h_x^2}{\alpha}\right). \tag{57}$$

An important result is that the enhanced gravity approach has embedded wavelike solutions as cnoidal waves and bores. This result allows for the use of the analytical methods of water wave theories to investigate the behavior of basic, simplified solutions for the flow of granular material. Evidently, *Denlinger and Iverson* [2004] proposed the first *Boussinesq-type* model for granular media but without exploiting it any further.

5. Exploratory Examples

5.1. General

In this section analytical results of the water wave theory will be applied to the motion of dry granular materials. The existence of simplified analytical solutions embedded into the general unsteady flow equations of dry granular material over a 3-D terrain has important implications. First, the simplified analytical solutions allow for an inspection of a specific model component, i.e., the nonhydrostatic or the dispersion portion. These particular solutions may not be directly found in nature, but they are particular solutions of a general model to understand the behavior of its physics. Second, simplified analytical solutions apply as test cases for numerical solutions of the full system of equations. It is difficult to evaluate the accuracy of a numerical code in unsteady flow over 3-D terrain, if analytical solutions are not available. However, under simplified and controlled flow conditions, it is possible to investigate how a numerical solver behaves, before expanding it to simulations in nature. This has been a traditional practice in hydraulic research, where, e.g., the analytical solitary wave solution [*Hager and Hutter*, 1984a, 1984b; *Sander and Hutter*, 1991; *Sander and Hager*, 1991] was used as test case for comparison of solitary wave predictions using numerical solvers of the full system of equations [*Sander and Hutter*, 1992; *Carmo et al*., 1993; *Kim et al*., 2009].

In this section, the ideal case of wavelike mass motion, denominated "*pseudouniform flow*" [*Hager and Hutter*, 1984b], is considered. In multidimensional flow this ideal case implies that the source term vector of the depth-averaged model vanishes, $\mathbf{S} = \mathbf{0}$. It does not mean horizontal topography; it rather implies the idealistic situation in which the basal slope driving components are exactly balanced by resistive forces, leading for 1-D depth-averaged flow to the system

$$\frac{\partial \mathbf{U}}{\partial t} + \frac{\partial \mathbf{F}}{\partial x} = \mathbf{0}, \quad \mathbf{U} = \begin{pmatrix} h \\ Uh \end{pmatrix}, \quad \mathbf{F} = \begin{pmatrix} Uh \\ M \end{pmatrix}. \tag{58}$$

In addition, the flow over variable topography will be considered to make a clear distinction between the material free surface and the basal stress line originating from the higher-order wave theory presented herein. For that, the illustrative and basic test case of flow over a Gaussian hump under isotropic, steady flow will be considered, for which topographic source terms must be accounted for.

5.2. Granular Solitary Wave

Consider a translation wave in the x direction with constant propagation speed c. Using the change of variables $X = x - ct$, $T = t$ (a Galilean transformation) these waves appear steady in a moving system of

reference, given that the constant c implies a wave profile that is not deformed [*Serre*, 1953; *Iwasa*, 1955; *Liggett*, 1994]. Thus, under such pseudouniform flow conditions, the governing equations reduce to

$$\frac{\partial}{\partial X}(\mathbf{F} - c\mathbf{U}) = \mathbf{0}, \tag{59}$$

implying that the momentum in the moving reference system is conserved, i.e., (viz., $(26)_1$, middle equation)

$$U^2 h - cUh + \frac{1}{\rho} K \int_{z_b}^{z_s} \tau_{zz} \mathrm{d}\varsigma = \text{const}. \tag{60}$$

The mass (volume) balance equation yields the constant progressive discharge $q = (U - c)h$ (viz., $(26)_1$, top equation). Using equation (36) for τ_{zz}, inserting it into equation (60), and using the definition of the progressive discharge gives

$$Kg\frac{h^2}{2} + \frac{q^2}{h}\left(1 + K\frac{hh_{XX} - h_X^2}{3}\right) = \text{const}. \tag{61}$$

Thus, wave solutions are generally given by the integrals of

$$Kg\frac{h^2}{2} + \frac{q^2}{h}\left(1 + K\frac{hh_{XX} - h_X^2}{\alpha}\right) = \text{const} = M_o, \tag{62}$$

where M_o is the invariant momentum along the moving axis. Here $\alpha = 3$ for the general depth-averaged theory [*Serre*, 1953; *Benjamin and Lighthill*, 1954; *Iwasa*, 1955; *Hager and Hutter*, 1984b] and $\alpha = 4$ for the enhanced gravity approach [*Denlinger and Iverson*, 2004]. Let $\sigma = h_X{}^2$ be an auxiliary variable; with it, equation (62) is rewritten with $\lambda = 3\,K/\alpha$ as

$$\lambda\frac{q^2}{6g}h^2\frac{\mathrm{d}}{\mathrm{d}h}\left(\frac{\sigma}{h^2}\right) = \frac{M_o}{g} - K\frac{h^2}{2} - \frac{q^2}{gh}. \tag{63}$$

Equation (63) is integrated with respect to h which yields

$$\lambda\frac{q^2}{6g}h_X^2 = -\frac{M_o}{g}h - K\frac{h^3}{2} + \frac{q^2}{2g} + Ch^2. \tag{64}$$

Here C is a constant of integration, determined by imposing the solitary wave boundary conditions at $x \to \pm\infty$, namely, $h_X \to 0$ for $h \to h_o$, with h_o as the uniform flow depth. Note that $M_o = gKh_o{}^2/2 + q^2/(h_o)$. Using this in equation (64), the constant C equals $C = Kh_o + q^2/(2gh_o{}^2)$. Equation (64) is, therefore, rewritten as

$$h_X^2 = \frac{3}{\lambda \mathrm{F}_o^2}\left(-Ky^3 + \left(2K + \mathrm{F}_o^2\right)y^2 - \left(K + 2\mathrm{F}_o^2\right)y + \mathrm{F}_o^2\right) = \frac{3}{\lambda \mathrm{F}_o^2}\left((y-1)^2\left(\mathrm{F}_o^2 - Ky\right)\right), \tag{65}$$

in which $y = h/h_o$, and $\mathrm{F}_o = q(gh_o{}^3)^{-1/2}$ = undisturbed Froude number. If the left-hand side is also written in dimensionless form it assumes with $\chi = x/x_o$ and $x_o = 2\mathrm{F}_o h_o[3(\mathrm{F}_o{}^2 - 1)]^{-1/2}$ the form

$$\left(\frac{\mathrm{d}y}{\mathrm{d}\chi}\right)^2 = \frac{4}{\lambda\left(\mathrm{F}_o^2 - 1\right)}(y-1)^2\left(\mathrm{F}_o^2 - Ky\right). \tag{66}$$

Consider as a first case a dry granular solitary wave with isotropic stresses, with $K = \tau_{xx}/\tau_{zz} = 1$, which is identical to the clear-water flow. Solitary wave solutions of equation (66) are given by the following analytical family of solutions [*Serre*, 1953]

$$Y = \frac{y-1}{\left(\mathrm{F}_o^2 - 1\right)} = \mathrm{sech}^2\left[(\alpha/3)^{1/2}\chi\right], \tag{67}$$

in which $\lambda = 3/\alpha$ and $Y = (y-1)/(y_{\max} - 1)$ were used. Parameter α determines the solitary wave profile. Equation (67) is plotted in Figure 2 for $\alpha = 3$ and 4 and compared with solitary water wave laboratory data [*Naheer*, 1978]. Figure 2 indicates that the solution for $\alpha = 3$ is generally closer to experimental data than that for $\alpha = 4$. The solution of the solitary wave profile, equation (67), coincides with the classical Boussinesq solution invoking a sech^2 function [*Hager and Hutter*, 1984b; *Sander and Hager*, 1991]. However, the analytical solution includes a term given by F_o in $x_o = 2\mathrm{F}_o h_o[3(\mathrm{F}_o{}^2 - 1)]^{-1/2}$, not accounted for by the classical Boussinesq theory, which is less accurate upon comparison with the present results.

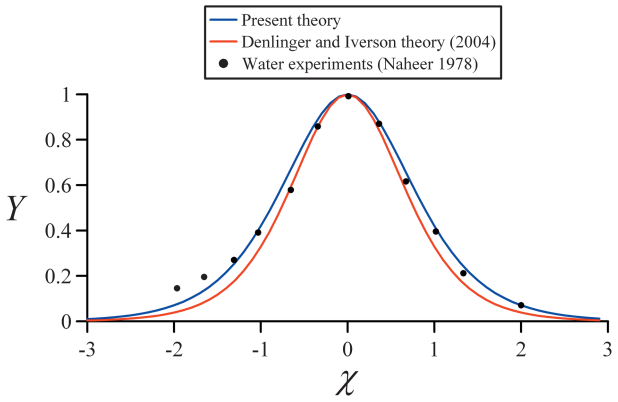

Figure 2. Family of granular solitary waves for isotropic stresses deduced by proposed model and compared with *Denlinger and Iverson* [2004] model.

The earth pressure coefficient K generally does not imply isotropic stresses. From the Mohr-Coulomb criterion, it is given by equation (41b). For a derivation see *Pudasaini and Hutter* [2007], or *Savage and Hutter* [1989]; there are also other formulae available, which then imply differently used stress anisotropies. Coefficient K equals the passive earth coefficient (plus sign in equation (41b) for a granular medium in compression, whereas it is taken as the active earth pressure coefficient for a dilated mass. However, the solitary wave solution requires a unique constant value for K. To model the solitary wave with anisotropic stresses the ideal situation of maximum bed roughness ($\phi_{bed} = \phi_{int}$) applies so that K has a unique value from equation (41b) given by

$$K_{act/pas} = \frac{1 + \sin^2\phi_{int}}{1 - \sin^2\phi_{int}}. \tag{68}$$

Equation (66) was solved numerically using the fourth-order Runge-Kutta method [*Press et al.*, 2007] for $\alpha = 3$ and $\alpha = 4$ (Figure 3), using $\phi_{bed} = \phi_{int} = 30°$ so that $K = 1.667$ from equation (68). The results confirm that the solutions are notably different, depending on the α value. In addition, the sensitivity of the wave profile on K is highlighted, given the significant variations as compared with the former isotropic computations. The maximum solitary wave height is $y_{max} = F_o^2/K$ from equation (66). Solitary waves are damped for the limiting case $K = F_o^2$, for which the flow profile, therefore, implies uniform flow conditions [$h(x) = h_o$].

The above procedure gives rise to construct from equation (64) an entire series of granular solitary wave solutions, in which the real axis $x \in \mathbb{R}$ is divided into regimes, with dilatational ($\partial U/\partial x > 0$) and compressive ($\partial U/\partial x < 0$) flows, respectively. For instance, the dilative solution of equation (64) with $K = K_{act}$ in $x \in (-\infty, x_{sep}]$ may be discontinuously connected with a solution having $K = K_{pas}$ for $x \in [x_{sep}, \infty)$. The transition conditions at x_{sep} must thereby satisfy the Rankine-Hugoniot (= mass and momentum jump) conditions of the granular material. These solutions describe granular shocks and may be generated for a dry granular layer flowing on a bed with a small hump. However, the equations in this section do not apply since $z_b = 0$ has been assumed.

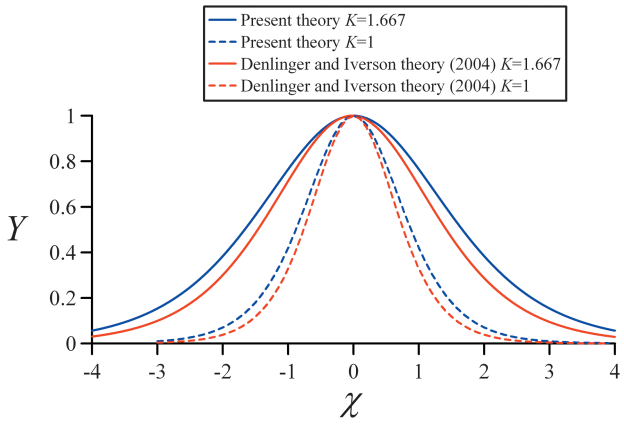

Figure 3. Family of granular solitary waves for anisotropic stresses deduced by proposed model and compared with *Denlinger and Iverson* [2004] model.

5.3. Granular Fall

Consider a steady state case under pseudouniform flow conditions, namely, the free overfall [*Hager*, 1983; *Marchi*, 1992, 1993]. It occurs in a straight-bottomed flume abruptly ending in a free fall, where the upstream mass flow separates, continuing as a free jet. It is well known from open channel hydraulics that changes in nonhydrostatic pressure are intensified under rapid variations of the bed geometry [*Hager and Hutter*, 1984a; *Matthew*, 1991; *Montes*, 1998]. This test case highlights how the granular flow behaves in response to vertical accelerations when abrupt changes in topography play a significant role. The flow

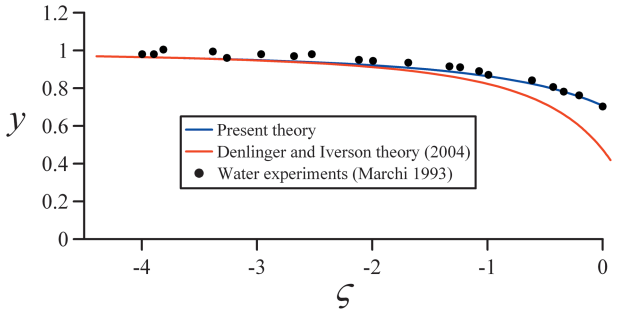

Figure 4. Family of granular free overfalls for isotropic stresses deduced by proposed model and compared with *Denlinger and Iverson* [2004] model.

in the upstream free overfall portion has attracted a number of studies to analyze the effects of vertical acceleration. A typical case is the free overfall with critical approach flow conditions $F_o = 1$ [*Hager*, 1983]. Equation (66) is singular in this case, so that it must be rescaled with

$$y = \frac{h}{h_c}, \quad \varsigma = \frac{x}{h_c}, \quad h_c = \left(\frac{q^2}{g}\right)^{1/3}. \tag{69}$$

With these scales the singularity is removed; the equation analogous to equation (66) states

$$\left(\frac{dy}{d\varsigma}\right)^2 = \frac{3}{\lambda}(y-1)^2(1-Ky). \tag{70}$$

Consider a dry granular free overfall with isotropic stresses $K = 1$. Note the full analogy with clear-water flow, from which equation (70) integrates to

$$\varsigma = 2\left(\frac{\lambda}{3}\right)^{1/2}(1-y)^{-1/2} + C. \tag{71}$$

For $\lambda = 1$ ($\alpha = 3$) this equation was obtained by *Hager* [1983] for clear-water flow. Equation (71) is plotted in Figure 4 for $\alpha = 3$ using as boundary condition to compute C the point $y(-3.5) = 0.958$. The computed free surface profile excellently compares with the data of *Marchi* [1993]. The solution for $\alpha = 4$ and the same boundary condition is also plotted to highlight the effect of α. Significant variations result in this case, indicating the sensitivity to this factor near extreme changes of the basal geometry.

If $K \neq 1$, the general solution of equation (70) reads [*Bronshtein and Semendiaev*, 1971, chap. III, pp. 385–404]

$$\left(\frac{3}{\lambda}\right)^{1/2}\varsigma + C = (1-K)^{-1/2}\ln\left[\frac{(1-Ky)^{1/2} - (1-K)^{1/2}}{(1-Ky)^{1/2} + (1-K)^{1/2}}\right]. \tag{72}$$

For flow approaching a free fall, the grain particles are under an active tension state, so that K is given by the active earth coefficient ($K < 1$). A value of $K = 0.6$ was considered with equation (72) plotted in Figure 5 for $\alpha = 3$ and 4 using the point $y(-3.5) = 0.998$ as boundary condition to compute C. Results indicate that the solutions for $\alpha = 3$ and $\alpha = 4$ significantly deviate as the fall is approached. The same case was also solved using $K = 0.75$, with the results also included in Figure 5. Note that moderate variations in K induce significant variations of the computed $y(0)$ for identical boundary conditions. Boussinesq-type wave solutions for flows over varying topography are thus sensitive to both the anisotropy of stresses and to the dispersion coefficient of the nonhydrostatic part of the model.

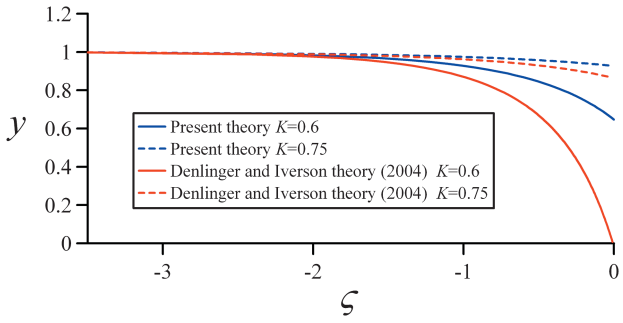

Figure 5. Family of granular free overfalls for anisotropic stresses deduced by proposed model and compared with *Denlinger and Iverson* [2004] model.

5.4. Flow Over a Hump

The flow over variable topography implies that the source term in equation (26) is not zero, i.e., resistive forces and bed geometrical source terms must be accounted for. In geophysical environments, the effect of variable topography on the flow solution of dynamical models stating conservation of mass and momentum is routinely tested using simplified bed

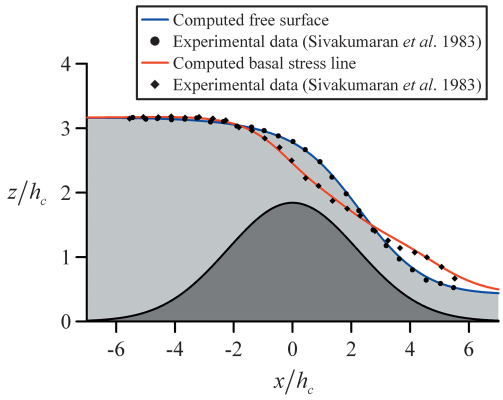

Figure 6. Free surface and basal piezometric stress (pressure) line in flow over a hump. Comparison of proposed model with experiments by *Sivakumaran et al.* [1983].

geometry forms [*Engelund and Hansen*, 1966; *Sivakumaran et al.*, 1983; *Sivakumaran and Dressler*, 1989]. One such form is the Gaussian hump

$$z_b = a\,\exp\left(-bx^2\right). \tag{73}$$

A simple and smooth analytical bed shape can be used to emulate the flow of atmospheric air currents over variable terrain [*Sivakumaran and Dressler*, 1989] or the water flow over bed forms like dunes and antidunes in a river [*Engelund and Hansen*, 1966; *Dey*, 2014]. In the context of granular flows, it is also an ideal test case to show how the higher-order Boussinesq theory incorporates differences between, namely, free surface and basal stresses in the flow solution. In the 3-D unsteady numerical tests by *Denlinger and Iverson* [2004] the flow is computed over an irregular topography; there, it is more difficult to show and compare different elements of the theory. However, over a simple bed geometry it is possible to highlight with elementary computations a key element of the theory: the nonhydrostatic dispersion term. In what follows, isotropic stresses are assumed ($K=1$) and resistive forces are neglected. These can be easily incorporated in the numerical computations described below. Here the simplest computations are done for illustrative purposes. For 1-D steady flow over variable topography the Boussinesq momentum model gives the set of ordinary differential equations (ODEs) (Appendix D)

$$\frac{\mathrm{d}M}{\mathrm{d}x} = -\frac{(\tau_{zz})_b}{\rho}\frac{\partial z_b}{\partial x}, \quad M = g\frac{h^2}{2} + hU^2\left(1 + \frac{hh_{xx} - h_x^2}{3} + \frac{hz_{bxx}}{2} - \frac{h_x z_{bx}}{2}\right), \tag{74}$$

where the basal stress is (Appendix D)

$$\frac{(\tau_{zz})_b}{\rho g} = h + \frac{U^2}{2g}\left[2hz_{bxx} + hh_{xx} - h_x^2 - 2h_x z_{bx}\right]. \tag{75}$$

Figure 6 contains the water experimental measurements of *Sivakumaran et al.* [1983] for a Gaussian hump of profile $z_b = 20\exp[-0.5(x/24)^2]$ (cm). The water discharge is 0.11197 m^2/s (critical depth $h_c = 0.1085$ m). The figure shows the measured free surface and bed stress piezometric (pressure) lines. The clear divergence between the two indicates the effect of the vertical acceleration as the flow passes from subcritical to supercritical conditions. Equations (74) and (75) can be written as a system of three ODEs for the unknowns $M(x)$, $h(x)$, and $h_x(x)$ over variable topography. The system was solved herein using the fourth-order Runge-Kutta routine by *Press et al.* [2007]. For the solution, the following iteration process was adopted. First, a value of h was guessed at an inflow section where computations initiate far from extreme topographic changes, whereby the flow is hydrostatic. This section was taken at a distance of 10 critical depths from the crest. The water surface slope there was set to zero, and M was computed as for hydrostatic flows using this value of h. The system of ODEs was then numerically solved. If the initial value of h is incorrect, then the flow is not able to cross the hump and the computed depth goes to zero elsewhere. The value of h is then iterated until the flow passes the hump and at a section away from the crest a surface slope close to zero is reached. The computational results are depicted in Figure 6, with all quantities normalized by the critical depth h_c. The comparison of computed and measured quantities is good; it highlights a key ingredient of the Boussinesq theory: differences between free surface and bed stress piezometric lines are correctly accounted for. If the same flow is computed using a pure Saint-Venant theory the free surface is not accurately predicted, given that the vertical acceleration is not accounted for, whereas the bottom pressure can simply not be predicted. This is a strong reason to adopt the higher-order Boussinesq theory in geophysical environments, given that the increase of computational efforts is small, and the gain in physical accuracy high.

6. Flow Over Curved Terrain: Cartesian Versus Curvilinear Coordinates

Use of basal-fitted coordinates as in *Hutter and Savage* [1988], *Gray et al.* [1999], or *Iverson and Denlinger* [2001] to formulate mass and momentum equations was earlier introduced by *Dressler* [1978] for water wave

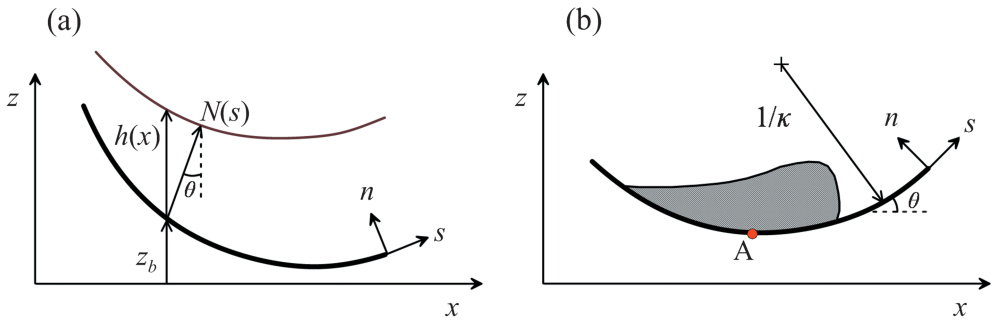

Figure 7. Cartesian versus curvilinear coordinates in curved terrain; (a) definition of flow depth; (b) pressures at point A.

problems. In this formulation the nonhydrostatic stress normal to the bed is proportional to the local basal curvature κ, physically representing centripetal forces. This nonhydrostatic effect to the momentum equation is *due to the curvilinearity of the coordinate system* and survives in the lowest order shallowness approximation, in which the classical shallow flow theory, referred to Cartesian coordinates, produces a hydrostatic force balance from the momentum balance law perpendicular to the basal surface. This contribution is of differential geometric origin of the Riemannian metric, which does not arise when a Cartesian frame is used. Contrary to this, the Boussinesq-like [*Serre*, 1953; *Matthew*, 1991; *Kim et al*., 2009] equations, addressed in this work, account for local and convective vertical accelerations (irrespective whether this is flat or curved) in the depth distribution of the pressure τ_{zz} (see, e.g., equation (34)). This contribution is of *dynamic* or *physical origin* and says that the perturbation analysis of *Savage and Hutter* [1989] and others goes too far in pursuing the limit as the shallowness parameter becomes small. In general, when dynamical equations are written in a curvilinear coordinate setting, both effects ought to be accounted for. Even though it appears that the curvature contribution to the basal pressure is somewhat smaller than the enhanced gravity contribution by *Denlinger and Iverson* [2004], the issue or recommendation is not to drop the former against the latter. Both must be considered and software for natural topography amended by adding the enhanced gravity term as proposed by *Denlinger and Iverson* [2004].

For illustrative purposes of the differences between both sets of coordinates consider 2-D plane flow, with Cartesian coordinates (x, z) and orthogonal curvilinear coordinates fitted to terrain (s, n) (Figure 7a). At a given section the Cartesian flow depth measured in the z direction is $h(x)$, whereas in curvilinear coordinates the flow depth measured in the n direction is $N(s)$. With θ as the local bed inclination at any section (with corresponding x and s coordinates), the projected vertical flow depth h on the bed-normal direction, $h\cos\theta$, is, in general, different from the normal flow depth N, given the appreciable curvature and inclination of the material free surface. Consider now a concave bed terrain and a granular mass flow at a given instant of time (Figure 7b). An illustrative case following *Hager* [2010] assumes the steady state flow equations at this instant. Stresses in the n direction (τ_{nn}) or the z direction (τ_{zz}) are important for the computation of the flow momentum M and the basal resistive force in the (x, z) and (s, n) reference systems, respectively. The local basal angle with the horizontal θ and the bed curvature κ are geometrically related as $\kappa = \mathrm{d}\theta/\mathrm{d}s$. The stress distribution in the n direction is then given by [*Savage and Hutter*, 1991]

$$\tau_{nn} = \rho g(N-n)\cos\theta + \rho\kappa\int_n^N \frac{u_s^2}{1+\kappa n}\mathrm{d}\xi. \tag{76}$$

Here u_s is the velocity in the s direction. If u_s is replaced by a depth-averaged value U_s, and shallow flow is considered ($\kappa n << 1$), equation (76) reads for the basal stress

$$(\tau_{nn})_b = \rho g N\cos\theta + \rho U_s^2 \ln(1+\kappa N) \approx \rho g N\cos\theta + \rho\kappa N U_s^2. \tag{77}$$

This is the centripetal correction used by *Iverson and Denlinger* [2001] to enhance the basal resistive force computation. The enhanced gravity for this case of steady 1-D flow over curved terrain is

$$g' = g + \frac{D\overline{w}}{Dt} = g + U\frac{\partial\overline{w}}{\partial x}, \tag{78}$$

and, from equations (7), (8), and (47),

$$\overline{w} = \frac{1}{2}(w_s + w_b) = \frac{1}{2}\{U(h_x + z_{bx}) + Uz_{bx}\}. \tag{79}$$

Differentiation of equation (79) produces

$$\frac{\partial \overline{w}}{\partial x} = U_x\left(\frac{h_x}{2} + z_{bx}\right) + U\left(\frac{h_{xx}}{2} + z_{bxx}\right). \tag{80}$$

Inserting equation (80) into equation (78), using the expression $U_x = -q/h^2 h_x$, and inserting the resulting g' into equation (48), yields the basal vertical tension of the *Denlinger and Iverson* [2004] theory for this flow problem as

$$(\tau_{zz})_b = \rho g h + \rho \frac{U^2}{2}\left(hh_{xx} - h_x^2 - 2h_x z_{bx} + 2hz_{bxx}\right). \tag{81}$$

Equation (81) was first derived by *Castro-Orgaz and Hager* [2009] for channel flow structures and is identical to equation (D7) for the generalized Boussinesq theory derived herein (Appendix D). At an extremum of the basal line (point A in Figure 7b) $z_{bx} = 0$, $\theta = 0$, and thus, $h = N$. Thus, equations (77) and (81) are directly comparable. Equation (77) involves only the differential geometric curvature effect, but equation (81) contains two effects, those due to curvilinearity of the bed profile $z = z_b(s)$ or $z = z_b(x)$, and due to the dynamical variation of h with x coordinate. Stresses are proportional to $z_{bxx} = \kappa$ in the curvilinear equation (77), whereas the Cartesian equation (81) contains terms involving h_x and h_{xx} in addition. A consequence is that the equations of *Iverson and Denlinger* [2001] do not admit nonhydrostatic wave solutions over a planar surface. In contrast, their 2004 Cartesian formulations account for both effects of h_x and h_{xx} and, thus, model the nonhydrostatic pressure field in greater detail. If $h_x = h_{xx} \approx 0$, both models converge at point A to

$$(\tau_{zz})_b \approx (\tau_{nn})_b \approx \rho g h + \rho U^2 h z_{bxx}. \tag{82}$$

However, this is not general and illustrates that the two models produce different results. In conclusion, because the models with enhanced normal acceleration contributions tend to yield results in better agreement with data, models not accounting for them need to be amended.

In general, both systems of coordinates (x, z) and (s, n) can be used to model flow over highly curved and steep terrain. The standard hydrostatic Saint-Venant theory in Cartesian coordinates gives poor results over variable topography [*Dressler*, 1978], whereas the nonhydrostatic Boussinesq theory presented in this work can give very accurate results with a small increase in computational complexities. The equivalents to the Saint-Venant equations in curvilinear coordinates (s, n) are the so-called Dressler equations in the water environment. The equivalents to these equations for avalanches are widely used by granular flow workers [i.e., *Iverson and Denlinger*, 2001]. These flow equations can give good results for flow over variable terrain, given that the curvilinear formulation of the mass and momentum equations introduces a geometric effect that permits to model nonhydrostatic pressure at the lowest order of asymptotic expansion [*Dressler*, 1978]. However, the equations are physically relevant only if the material free surface is locally parallel to the bed surface (local concentric streamlines), such that spatial derivatives of the depth N, i.e., $\partial N/\partial s$ and $\partial^2 N/\partial s^2$ can be neglected [*Hager*, 2010]. This is the price of using the n direction as preferential spatial coordinate for doing a Saint-Venant-type depth averaging. Thus, Dressler-type (or curvilinear Saint-Venant-type) equations cannot give wavelike solutions over planar surfaces or horizontal beds, and, as further found in the water literature, would have limited performance on concave beds, where physical solutions are limited to the constraint $N\kappa < 1$; that is, the determinant of the Jacobian matrix must be positive [*Dressler*, 1978]. A distinctive feature of Dressler-type equations is that they are mathematically much more complex than the equivalent Saint-Venant equations for Cartesian coordinates. As to higher-order Boussinesq-type equations the same can be stated; a Boussinesq theory can also be developed for curvilinear coordinates accounting for terms like $\partial N/\partial s$ and $\partial^2 N/\partial s^2$, but the results would be mathematically more complex than the Cartesian model developed herein. For that reason, we presented here the general Boussinesq theory in the Cartesian

framework, but we give all the elements of the theory so that a germane development could be done by the granular community in curvilinear coordinates, if found necessary. However, the mathematical complexities are not trivial.

7. Numerical Treatment of Boussinesq-Type Models

A simulation of unsteady flow over 3-D terrain using shallow flow models generally requires numerical solutions. The numerical technique used to solve the mathematical equations describing the physical system must be robust and stable. Flow over irregular topography will experience changes in flow regimes with the developments of moving shocks [*Vreugdenhil*, 1994; *Toro*, 1997, 2002; *Chaudhry*, 2008; *Kim et al*., 2009]. A first key issue for numerical modeling is that the system of equations must be written in conservative form, as done in equation (26). Otherwise shocks are not captured. Among current numerical methods the finite volume is possibly the most successful in free surface flow modeling [*LeVeque*, 2002; *Kim et al*., 2009; *Tai et al*., 2012; *Kuo et al*., 2009, 2010, 2011] although it is sometimes coupled in a hybrid fashion with finite-difference and finite element methods. Models are generally explicit and constrained by the Courant-Friedrichs-Lewy condition for the time step Δt. Computations comprise reconstruction (e.g., linear and parabolic) of the vector **U** of conserved variables at a given time level using known cell-averaged values. A variety of methods for flux (**F**, **G**) computation is available, but approximate Riemann solvers HLL and HLLC generally dominate [*Guinot*, 2003]. Slope limiters as minmod or superbee [*Toro*, 2002] are used to minimize spurious oscillations in the solution. Once numerical fluxes are computed with the Riemann solver based on the reconstructed solution, time stepping is done with an Euler approximation for the mean $\partial \mathbf{U}/\partial t$ over a cell. Source term effects are then incorporated in the solution using any method to solve ODEs, like Euler or the more accurate Runge-Kutta methods [*Toro*, 2002]. This summarizes the straightforward sequence for coding a shallow flow model if vertical stresses are hydrostatic. This is essentially the method used by *Denlinger and O'Connell* [2008] in their shallow flow model enhanced to account for a mean vertical velocity component. However, experience in water wave modeling revealed that if dispersion effects are introduced in the system by using equations (29) and (32), an improved treatment may be advisable.

For illustrative purposes of the numerical difficulties introduced by dispersion terms, consider equations (37) and (38). Assume that they are discretized using finite differences. Finite differencing to second-order accuracy of first-order derivatives in the Saint-Venant terms produces truncation errors proportional to U_{xx} and U_x. These errors will have mathematically the same form as the physical dispersive terms [*Abbott*, 1979; *Wei and Kirby*, 1995]. Slope limiters in finite volume methods are introduced to eliminate spurious oscillations originating from steep gradients near shocks. If no account is made to differentiate truncation errors from physical dispersive terms, not only numerical oscillations may be damped out but also physical components. Thus, higher-order differencing of leading order hydrostatic terms is required to guarantee that physical dispersion effects are not masked by spurious numerical oscillations associated with truncation errors [*Wei and Kirby*, 1995]. Ideally, these problems disappear with a computational mesh where $\Delta x \rightarrow 0$ and $\Delta y \rightarrow 0$. However, this is unpractical so that the control of truncation errors is necessary for usual meshes.

Kim et al. [2009] provide a useful reference, given the account of all these issues in a finite volume model. Their modified finite volume method for dispersive systems consists in substituting the Euler time stepping by a fourth-order accurate time stepping method, composed of a predictor step using a third-order Adams-Bashforth formula and an iterative corrector using a fourth-order Adam-Moulton formula. The treatment of the leading order hydrostatic terms was done using a fourth-order accurate MUSCL TVD for reconstruction of interface values and a HLLC Riemann solver to compute fluxes. Prior to the application of the finite volume solution, vector **U** is mathematically substituted by an auxiliary vector that includes terms with spatial derivatives. This is done to eliminate time derivatives (contained in mixed terms like U_{xt}) from the vectors **F** and **G**. Solution is then performed for auxiliary variables and the vector **U** is determined by discretizing the spatial derivatives to second-order accuracy, leading to tridiagonal systems for determining **U**. This method appears useful for future implementation in physical granular flow models, like in *Denlinger and Iverson* [2004]. Refinement of numerical treatment of dispersive systems in water wave modeling lasted decades, and a significant effort is still needed to investigate these issues in debris flow modeling. As indicated by *Iverson* [2014], these efforts only start, and this review may indicate a new look for future development of debris flow numerical solvers.

8. Conclusions

Mathematical modeling of granular mass flows is performed using Saint-Venant-type mass and momentum, depth-averaged, hydrostatic equations employing the continuum mechanics approach. However, vertical accelerations of the same order as the gravity acceleration, recently found in fully unsteady flow simulations of granular mass flow over three-dimensional terrain, indicates that mathematical modeling must be nonhydrostatic. This leads to the basic question of whether these geophysical flows are described by Boussinesq-type gravity waves, or not. The conclusion of this work is *yes*.

The fundamental depth-averaged Boussinesq-type gravity wave model used in hydraulic research for more than a century has been generalized for granular media, resulting in the following implications: We gave a full mathematical theory *free of ad hoc assumptions* that permits incorporation of nonhydrostatic stresses into depth-averaged models. The *increase of computational effort* of the higher-order theory developed over standard Saint-Venant type formulations is *small*, making the present theory suitable for wide adoption by granular flow workers. The *gain in physical accuracy* adopting the present theory *is large* as compared to standard Saint-Venant equations, given that geophysical flow conditions not amenable for solution using the latter theory, can be solved. Of course, the Boussinesq theory applies to all pertinent situations where the Saint-Venant theory can be used.

The present theory was compared with the enhanced gravity solver of *Denlinger and Iverson* [2004] that is based on several ad hoc *assumptions*: (i) Assumption of a mean vertical velocity taken as the average between free and basal material surface kinematic boundary conditions, (ii) use of a mean vertical acceleration based on that mean value of the vertical velocity, and (iii) use of a linear vertical stress profile. In contrast, in the present theory the vertical velocity, vertical acceleration, and vertical stresses are determined mathematically using mass and momentum conservation equations without any ad hoc simplification. Comparing our theory with that of *Denlinger and Iverson* [2004], we found that both give similar, but not identical, depth-averaged equations; in *Denlinger and Iverson*'s [2004] theory dispersion terms are affected by a different factor originating from the assumptions introduced into the vertical stress distribution.

Using the new analytical theory developed for the vertical velocity, the stress distribution, and acceleration terms are mathematically determined within the shallow flow approximation originating from scaling considerations. The theory is developed to facilitate its implementation and future enhancements within the context of the water wave theory.

Denlinger and Iverson [2004] presented a nonhydrostatic model for 3-D terrain that we reckon to be the first Boussinesq-type model proposed for granular media. Whereas they focused on the full numerical solution of nonhydrostatic dry granular flow over three-dimensional terrain using their model, we concentrated on the basic features of the new Boussinesq theory, obtaining analytical solutions of simplified flow cases. These solutions may not be real geophysical flows observed in nature; in contrast, the relevance of finding simplified analytical solutions is twofold: First, it provides a critical understanding of the fundamental core of the theory, the dispersion part; second, it allows for construction of basic analytical solutions to check the accuracy of numerical methods. It was found that the present theory results in a second-order differential equation for translation waves generalizing for granular media the *Benjamin and Lighthill* [1954] theory proposed for water waves. This is employed to obtain simplified analytical solutions of the full equations of motion including the solitary wave and the free overfall. It was found that the coefficient in the dispersion part of the model and the anisotropy of stresses are issues to which the model solution is sensitive near large changes in basal topography. Computations of flow over a hump, as typical in geophysical environment, revealed that the differences between the flow depth and the basal stress are large and must be accounted for over variable topography. It is shown that the Cartesian Boussinesq theory developed herein can account for these issues with little increase of complexities.

Consideration of the equations of motion into a curvilinear coordinate system revealed that beyond the enhanced gravity terms of the depth-averaged Boussinesq-type momentum equations in the Cartesian (x,y,z) system, normal pressure contributions due to centripetal-type acceleration led to a further enhancement of the pressure exerted at the basal bed. In general, the Boussinesq theory can be developed both in Cartesian and curvilinear coordinates, the latter system resulting in more complex mathematical expressions. Given that developments in a Cartesian framework are simpler, we presented these herein, facilitating the direct use of the theory by the granular community.

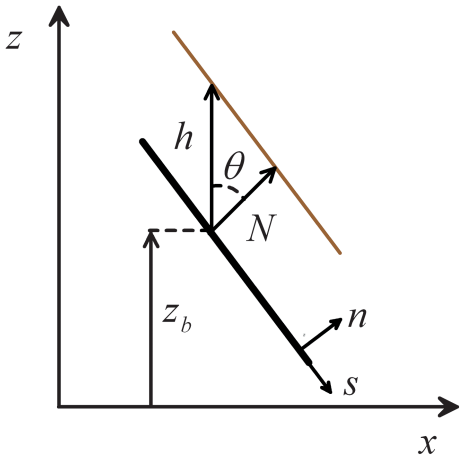

Figure A1. Cartesian- and terrain-fitted curvilinear coordinates for uniform flow on steep slope.

Appendix A: Order of Vertical Acceleration

Let $[x]$, $[y] = L$, and $[z] = H$ be horizontal and vertical scales in the Cartesian system of reference (x, y, z). Conservation of volume (mass if $\rho = \text{const}$) then implies for the velocity scales

$$\frac{[w]}{[u]} = \frac{[w]}{[v]} = \frac{H}{L} = \varepsilon. \tag{A1}$$

With the velocity $[u] = (gL)^{1/2}$ and time scalings $[t] = (L/g)^{1/2}$ one readily deduces

$$\frac{[\mathrm{d}w]}{[\mathrm{d}t]} = \varepsilon(Lg)^{1/2}(g/L)^{1/2} = \varepsilon g. \tag{A2}$$

For $\varepsilon \ll 1$, this result suggests that the vertical acceleration is asymptotically small as compared to g. In this case the terrain is not steep and the vertical momentum balance reduces to a hydrostatic pressure distribution. *Otherwise* the hydrostatic pressure assumption is invalid and vertical accelerations must be accounted for. It means that $\varepsilon = O(1)$ and that the terrain slopes $\partial z_b/\partial x$ and $\partial z_b/\partial y$ are steep. If the Cartesian coordinate system is inclined by an angle θ with respect to the gravitational direction then $[\mathrm{d}w/\mathrm{d}t] = g\varepsilon\cos\theta$, and with isotropic scaling ($\varepsilon = 1$), the bed-normal acceleration may be ignored for rapid gravity driven-flow on very steep mountain slopes. As an illustrative example consider the simplest case of uniform granular flow down a steep slope (Figure A1). In the curvilinear coordinates (s, n) following terrain the velocity is $U_s = q/N$ and the velocity in the n direction is zero, where q is the solid discharge and N the flow thickness measured normal to the bed. Now, consider horizontal-vertical Cartesian coordinates (x, z). The depth-averaged velocity in the x direction reads $U = q/h$, where h is the vertical flow depth. From the bed kinematic boundary condition the vertical velocity in the z direction is $w = U\partial z_b/\partial x$. The absolute velocity is then $V = (u^2 + w^2)^{1/2} = U(1 + \tan\theta^2)^{1/2}$. From the flow geometry of Figure A1 one has $N = h\cos\theta$, leading to $V = q/N$, that is identical to U_s. While in (s, n) coordinates only U_s is nonzero, in Cartesian coordinates (x, z) u and w are of similar order of magnitude. For example, on a steep slope of $\theta = 45°$ $u = w = q/h$. Note that a shallow flow thickness N cannot guarantee a small h ($h = N/\cos\theta$) on a steep slope, e.g., $\theta > 70°$. However, the assumptions $u = U$ and $v = V$ used in the nonhydrostatic model for steep terrain only imply that the contributions of the nonuniformity of u and v with z on the momentum balance in the x and y directions, respectively, are neglected. This contribution is expressed in depth-averaged models by Boussinesq-type velocity corrections coefficients as

$$\beta_x = \frac{\int_{z_b}^{z_s} u^2 \mathrm{d}\varsigma}{U^2 h}, \quad \beta_y = \frac{\int_{z_b}^{z_s} v^2 \mathrm{d}\varsigma}{V^2 h}, \quad \beta_{xy} = \frac{\int_{z_b}^{z_s} uv \mathrm{d}\varsigma}{UVh}. \tag{A3}$$

Their magnitude is usually close to unity so that they can be neglected for depth-averaged modeling [*Vreugdenhil*, 1994; *Toro*, 2002; *Denlinger and Iverson*, 2004; *Hutter et al.*, 2005].

Appendix B: Mixture Flow Equations

For a mixture of a number N of constituents, for which the constituent mass balance law has the form

$$\frac{\partial \rho_a}{\partial t} + \mathrm{div}(\rho_a \mathbf{V}_a) = \rho_a{}^+, \quad a = 1, 2, \ldots\ldots, N, \tag{B1}$$

the corresponding mass balance for the mixture is given by

$$\frac{\partial \rho}{\partial t} + \rho \mathrm{div}(\mathbf{V}_{\mathrm{bar}}) = 0, \quad \rho = \sum_a \rho_a, \quad \rho \mathbf{V}_{\mathrm{bar}} = \sum_a \rho_a \mathbf{V}_a. \tag{B2}$$

Here a is the identifier of the constituent and $(\rho_a, \mathbf{V}_a)$ are the constituent density, called *partial density*, and velocity. The mixture density and velocity are $(\rho, \mathbf{V}_{\mathrm{bar}})$, respectively. The velocity $\mathbf{V}_{\mathrm{bar}}$ is called the density weighted or *barycentric velocity*. The quantity $\rho_a{}^+$ is the mass production rate of constituent a.

In solid-fluid mixtures (e.g., of immiscible components) the volume fraction v_a is that part of the volume of a representative volume element which is filled by constituent a. If $\widetilde{\rho_a}$ is the true density, i.e., the mass density of the pure constituent a, then $\rho_a = v_a \widetilde{\rho_a}$. Consider a mixture satisfying the following conditions:

1. All components are density preserving, $\rho_a = \text{const}$, for all a.
2. Mixture is saturated: $\sum_a v_a = 1$, that is, the constituents fill the entire space.
3. All mass production rates are zero; ${\rho_a}^+ = 0$.

We note and stress this fact that for a mixture of which all constituents are density preserving, the mixture must not be volume preserving. For a mixture satisfying these constraints the mass balance (B1) can be divided by $\widetilde{\rho_a}$ to yield

$$\frac{\partial v_a}{\partial t} + \mathrm{div}(v_a \mathbf{V}_a) = 0. \tag{B3}$$

or after summation over all a, because of saturation, $\sum_a v_a = 1$

$$\mathrm{div}\left(\sum_a v_a \mathbf{V}_a\right) = 0. \tag{B4}$$

In analogy to the barycentric velocity (B2) one may now also define the *volume-weighted* mixture velocity

$$\mathbf{V}_{\mathrm{vol}} = \sum_a v_a \mathbf{V}_a. \tag{B5}$$

For mixtures satisfying the constraints (i)–(iii), the volume-weighted mixture velocity is, therefore, solenoidal. [*Chen and Tai*, 2008]. This is a convenient property and is the likely reason why modelers in geophysical mass flows use it as *the* mixture velocity [e.g., *Iverson*, 1997, 2005; *Andreotti et al*., 2013, and others].

Now the momentum equations

$$\rho \frac{\mathrm{d}\mathbf{V}_{\mathrm{bar}}}{\mathrm{d}t} = -\mathrm{div}\mathbf{T} + \rho \mathbf{g}, \tag{B6}$$

or equations (2)–(4), hold in this form only if the mixture velocity is defined as the barycentric velocity whose field is not solenoidal (the pore space can still vary with space and time). It follows that equations (1)–(4) cannot simultaneously hold unless pore space variations are ignored. Modelers do not seem to be sufficiently aware of this fact. We shall assume this for simplicity and reserve the more general case to a later work.

Appendix C: Vertical Velocity and Nonhydrostatic Stresses in Cartesian Coordinates for 3-D Terrain

Integrating equation (1) between z_b and an arbitrary elevation z yields

$$\int_{z_b}^{z} \left(\frac{\partial u}{\partial x} + \frac{\partial v}{\partial y} + \frac{\partial w}{\partial z}\right) \mathrm{d}\varsigma = 0, \tag{C1}$$

This can be rewritten as

$$w(z) - w(z_b) = -\int_{z_b}^{z} \left(\frac{\partial u}{\partial x} + \frac{\partial v}{\partial y}\right) \mathrm{d}\varsigma. \tag{C2}$$

Using Leibniz' rule results in

$$w(z) - w(z_b) = -\left[\frac{\partial}{\partial x}\int_{z_b}^{z} u \mathrm{d}\varsigma + \frac{\partial}{\partial y}\int_{z_b}^{z} v \mathrm{d}\varsigma + u_b \frac{\partial z_b}{\partial x} + v_b \frac{\partial z_b}{\partial y}\right]. \tag{C3}$$

Using the kinematic boundary condition at $z = z_b$ given by equation (8) finally gives

$$w(z) = \frac{\partial z_b}{\partial t} - \left[\frac{\partial}{\partial x}\int_{z_b}^{z} u \mathrm{d}\varsigma + \frac{\partial}{\partial y}\int_{z_b}^{z} v \mathrm{d}\varsigma\right]. \tag{C4}$$

For nonhydrostatic stresses we start with the integral relation between an arbitrary elevation and the free surface

$$\int_z^{z_s}\left(\frac{\partial w}{\partial t}+\frac{\partial w^2}{\partial z}+\frac{\partial (wu)}{\partial x}+\frac{\partial (wv)}{\partial y}\right)\mathrm{d}\varsigma=\int_z^{z_s}-\frac{1}{\rho}\left(\frac{\partial \tau_{zz}}{\partial z}+\frac{\partial \tau_{zx}}{\partial x}+\frac{\partial \tau_{zy}}{\partial y}+\rho g\right)\mathrm{d}\varsigma. \tag{C5}$$

Using Leibniz's rule in the left-hand side (LHS) of equation (C5) yields after using the free surface kinematic boundary condition given by equation (7)

$$\begin{aligned}&\frac{\partial}{\partial t}\int_z^{z_s} w\mathrm{d}\varsigma-w_s\frac{\partial z_s}{\partial t}+\frac{\partial}{\partial x}\int_z^{z_s} wu\mathrm{d}\varsigma-w_su_s\frac{\partial z_s}{\partial x}+\frac{\partial}{\partial y}\int_z^{z_s} wv\mathrm{d}\varsigma-w_sv_s\frac{\partial z_s}{\partial y}+w_s^2-w^2\\&=\frac{\partial}{\partial t}\int_z^{z_s} w\mathrm{d}\varsigma+\frac{\partial}{\partial x}\int_z^{z_s} wu\mathrm{d}\varsigma+\frac{\partial}{\partial y}\int_z^{z_s} wv\mathrm{d}\varsigma-w^2.\end{aligned} \tag{C6}$$

Integrating the right-hand side of equation (C5),

$$\int_z^{z_s}-\frac{1}{\rho}\left(\frac{\partial \tau_{zz}}{\partial z}+\frac{\partial \tau_{zx}}{\partial x}+\frac{\partial \tau_{zy}}{\partial y}+\rho g\right)\mathrm{d}\varsigma=\frac{1}{\rho}[\tau_{zz}(z)-\tau_{zz}(z_s)]-g(z_s-z)-\frac{1}{\rho}\int_z^{z_s}\left(\frac{\partial \tau_{zx}}{\partial x}+\frac{\partial \tau_{zy}}{\partial y}\right)\mathrm{d}\varsigma. \tag{C7}$$

Using the identities given by equations (C6) and (C7) one finally arrives at the general equation for the vertical distribution of nonhydrostatic stresses in steep and curved 3-D terrain as

$$\tau_{zz}(z)=\tau_{zz}(z_s)+\rho g(z_s-z)-\rho w^2+\rho\frac{\partial}{\partial t}\int_z^{z_s} w\mathrm{d}\varsigma+\rho\frac{\partial}{\partial x}\int_z^{z_s} wu\mathrm{d}\varsigma+\rho\frac{\partial}{\partial y}\int_z^{z_s} wv\mathrm{d}\varsigma+\int_z^{z_s}\left(\frac{\partial \tau_{xy}}{\partial y}+\frac{\partial \tau_{zx}}{\partial x}\right)\mathrm{d}\varsigma. \tag{C8}$$

As usual, a zero traction on the material surface implies $\tau_{zz}(z_s)=0$. The basal stress is from equation (C8)

$$(\tau_{zz})_b=\rho gh-\rho w_b^2+\left[\rho\frac{\partial}{\partial t}\int_z^{z_s} w\mathrm{d}\varsigma+\rho\frac{\partial}{\partial x}\int_z^{z_s} wu\mathrm{d}\varsigma+\rho\frac{\partial}{\partial y}\int_z^{z_s} wv\mathrm{d}\varsigma+\int_z^{z_s}\left(\frac{\partial \tau_{xy}}{\partial y}+\frac{\partial \tau_{zx}}{\partial x}\right)\mathrm{d}\varsigma\right]_{z=z_b}. \tag{C9}$$

Integrating directly equation (C5) from $z=z_b$ to $z=z_s$

$$\int_{z_b}^{z_s}\left(\frac{\partial w}{\partial t}+\frac{\partial w^2}{\partial z}+\frac{\partial (wu)}{\partial x}+\frac{\partial (wv)}{\partial y}\right)\mathrm{d}\varsigma=\int_{z_b}^{z_s}-\frac{1}{\rho}\left(\frac{\partial \tau_{zz}}{\partial z}+\frac{\partial \tau_{zx}}{\partial x}+\frac{\partial \tau_{zy}}{\partial y}+\rho g\right)\mathrm{d}\varsigma, \tag{C10}$$

which yields a more illustrative equation describing the basal stress. As a previous step, Leibniz's rule in the LHS of equation (C10) yields after using the free surface and bed kinematic boundary conditions, given by equations (7) and (8)

$$\begin{aligned}&\frac{\partial}{\partial t}\int_{z_b}^{z_s} w\mathrm{d}\varsigma-w_s\frac{\partial z_s}{\partial t}+w_b\frac{\partial z_b}{\partial t}+\frac{\partial}{\partial x}\int_{z_b}^{z_s} wu\mathrm{d}\varsigma-w_su_s\frac{\partial z_s}{\partial x}+w_bu_b\frac{\partial z_b}{\partial x}+\frac{\partial}{\partial y}\int_{z_b}^{z_s} wv\mathrm{d}\varsigma\\&-w_sv_s\frac{\partial z_s}{\partial y}+w_bv_b\frac{\partial z_b}{\partial y}+w_s^2-w_b^2=\frac{\partial}{\partial t}\int_{z_b}^{z_s} w\mathrm{d}\varsigma+\frac{\partial}{\partial x}\int_{z_b}^{z_s} wu\mathrm{d}\varsigma+\frac{\partial}{\partial y}\int_{z_b}^{z_s} wv\mathrm{d}\varsigma.\end{aligned} \tag{C11}$$

Using equation (C11) in equation (C10) yields, after using Leibniz's rule in the stress integral,

$$\begin{aligned}(\tau_{zz})_b=\rho gh&+\rho\frac{\partial}{\partial t}\int_{z_b}^{z_s} w\mathrm{d}\varsigma+\rho\frac{\partial}{\partial x}\int_{z_b}^{z_s} wu\mathrm{d}\varsigma+\rho\frac{\partial}{\partial y}\int_{z_b}^{z_s} wv\mathrm{d}\varsigma+\frac{\partial}{\partial x}\int_{z_b}^{z_s}\tau_{zx}\mathrm{d}\varsigma+\frac{\partial}{\partial y}\int_{z_b}^{z_s}\tau_{zy}\mathrm{d}\varsigma+(\tau_{zx})_b\frac{\partial z_b}{\partial x}\\&+(\tau_{zy})_b\frac{\partial z_b}{\partial y}.\end{aligned} \tag{C12}$$

From equation (C12) it is observed that the basal stress $(\tau_{zz})_b$ is, in general, different from the static weight of the granular mass (ρgh). Differences stem from terms related to local ($\partial w/\partial t$) and convective ($\partial w/\partial x$ and $\partial w/\partial y$) accelerations, as well as from stresses within the flowing mass, and acting on the basal surface. Note, therefore, that the existence of a basal resistive force on steep terrain ($\partial z_b/\partial x$ and $\partial z_b/\partial y$ are $O(1)$) invalidates the

hydrostatic approach $(\tau_{zz})_b = \rho g h$, even if the flow is not accelerated ($\partial w/\partial t = \partial w/\partial x = \partial w/\partial y = 0$), e.g., in the simple case of uniform flow on a steep slope presented in Figure A1. Thus, the Saint-Venant theory cannot be applied for steep and curved terrain. To illustrate the role of stresses in generating nonhydrostatic pressures on steep terrain consider turbulent water flow in the vertical plane (x, z) of Figure A1. Neglecting viscous contributions, the stress tensor is then $\tau_{xx} = p - \sigma_{xx}$, $\tau_{zz} = p - \sigma_{zz}$ and $\tau_{xz} = -\sigma_{xz}$, where σ denotes the turbulent Reynolds stress due to time averaging of the Navier-Stokes equations for fluid flow. The 2-D vertically integrated x momentum equation for turbulent water flow is, from equation (13),

$$\frac{\partial}{\partial t}(Uh) + \frac{\partial}{\partial x}\left(U^2 h\right) = -\frac{1}{\rho}\left[\frac{\partial}{\partial x}\int_{z_b}^{z_s}(p - \sigma_{xx})\mathrm{d}\varsigma + (p - \sigma_{xx})_b\frac{\partial z_b}{\partial x} + (\sigma_{xz})_b\right]. \tag{C13}$$

An equation describing bottom pressure is found from equation (C12)

$$\frac{\partial}{\partial t}(\overline{w}h) + \frac{\partial}{\partial x}(\overline{w}Uh) = \frac{1}{\rho}\left[(p - \sigma_{zz})_b + \frac{\partial}{\partial x}\int_{z_b}^{z_s}\sigma_{xz}\mathrm{d}\varsigma + (\sigma_{xz})_b\frac{\partial z_b}{\partial x}\right] - gh. \tag{C14}$$

Here the depth-averaged vertical velocity is

$$\overline{w}(x, y, t) = \frac{1}{h}\int_{z_b}^{z_s} w\mathrm{d}\varsigma. \tag{C15}$$

For uniform flow on a steep slope (Figure A1) equation (C13) reduces to the x momentum balance

$$(p - \sigma_{xx})_b\frac{\partial z_b}{\partial x} + (\sigma_{xz})_b = 0. \tag{C16}$$

In turn, the z momentum balance is from equation (C14)

$$(p - \sigma_{zz})_b + (\sigma_{xz})_b\frac{\partial z_b}{\partial x} = \rho g h. \tag{C17}$$

For a state of pure shear on the bed, the stress tensor at the bed simplifies to [*Steffler and Jin*, 1993]

$$\begin{aligned}(\sigma_{zz})_b &= 2\tau_b\cos\theta\sin\theta,\\ (\sigma_{xx})_b &= -2\tau_b\cos\theta\sin\theta,\\ (\sigma_{xz})_b &= \tau_b\left(\cos^2\theta - \sin^2\theta\right).\end{aligned} \tag{C18}$$

Here τ_b is the shear stress in the s direction, measured along the sloping plane (Figure A1). Inserting equation (C18) into equations (C16) and (C17) yields, respectively,

$$\tau_b = -p_b\tan\theta, \tag{C19}$$

$$p_b = \rho g h + \tau_b\tan\theta. \tag{C20}$$

Combining equations (C19) and (C20) results in the nonhydrostatic bottom pressure on a steep slope as

$$\frac{p_b}{\rho g} = \frac{h}{1 + \tan^2\theta} = h\cos^2\theta. \tag{C21}$$

Equation (C21) indicates that the bottom pressure on a steep slope is nonhydrostatic, which becomes important, for example, for $\theta = 45°$, resulting in a reduction of bottom pressure of 50% over the vertical water weight. Equation (C21) is a classical result obtained in the channel flow literature [*Chaudhry*, 2008]. However, equation (C21) is a particular nonhydrostatic result of the general formulation given by equation (C12). This development highlights that nonhydrostatic pressures on steep terrain may originate from stresses, and not from the vertical velocity $\overline{w}$, as in the simple uniform flow case presented for which the gradients $\partial\overline{w}/\partial x$ are zero.

Appendix D: One-Dimensional, Steady Momentum Model in Curved Terrain

The vertical velocity for steady 1-D flow over curved terrain is, from equation (29)

$$w = U\left[\frac{\partial z_b}{\partial x} + \frac{\partial h}{\partial x}\frac{(z - z_b)}{h}\right]. \tag{D1}$$

The vertical stresses are then given by equation (32) as

$$\tau_{zz}(z) = \rho g(z_s - z) - \rho w^2 + \rho \frac{\partial}{\partial x}\left(U \int_z^{z_s} w \mathrm{d}\varsigma\right). \tag{D2}$$

Inserting equation (D1) into equation (D2) gives after performing the integrals and derivatives

$$\frac{\tau_{zz}(z)}{\rho g} = h - \eta + \frac{U^2}{2g}\left[2hz_{bxx}\left(1 - \frac{\eta}{h}\right) + \left(hh_{xx} - h_x^2\right)\left(1 - \frac{\eta^2}{h^2}\right) - 2h_x z_{bx}\left(1 - \frac{\eta}{h}\right)\right]. \tag{D3}$$

In this case nonhydrostatic stresses over curved terrain originate from the convective acceleration. The flow momentum M is, for isotropic conditions ($K = 1$),

$$M = \int_{z_b}^{z_s}\left(u^2 + \frac{\tau_{zz}}{\rho}\right)\mathrm{d}\varsigma = hU^2 + \int_{z_b}^{z_s}\frac{\tau_{zz}}{\rho}\mathrm{d}\varsigma. \tag{D4}$$

Inserting equation (D3) gives, after integration,

$$M = g\frac{h^2}{2} + hU^2\left(1 + \frac{hh_{xx} - h_x^2}{3} + \frac{hz_{bxx}}{2} - \frac{h_x z_{bx}}{2}\right). \tag{D5}$$

Note that nonhydrostatic effects are given by both the spatial derivatives of the bed $z_b = z_b(x)$ and flow depth $h = h(x)$ profiles. The conservation momentum equation in the x direction retaining only bed slope source terms is, from equation (25),

$$\frac{\mathrm{d}M}{\mathrm{d}x} = -\frac{(\tau_{zz})_b}{\rho}\frac{\partial z_b}{\partial x}, \tag{D6}$$

where the basal stress is from equation (D3)

$$\frac{(\tau_{zz})_b}{\rho g} = h + \frac{U^2}{2g}\left[2hz_{bxx} + hh_{xx} - h_x^2 - 2h_x z_{bx}\right]. \tag{D7}$$

Acknowledgments

This work was supported by the Spanish projects CTM2013-45666-R and P09-AGR-4872. The work of K. Hutter was self-supported. Data supporting Figures 2, 4, and 6 are available in *Naheer* [1978], *Marchi* [1993], and *Sivakumaran et al.* [1983], respectively, as also acknowledged in the corresponding figure legends. The authors are grateful to the Chief Editor, A.L. Densmore, Associate Editor, and the three reviewers, who gave constructive detailed critiques that greatly improved our work. We would like to acknowledge that the main results and derivations of Appendix A of this work were generously offered by Yih-Chin Tai, National Cheng Kung University, Tainan, Taiwan.

References

Abbott, M. B. (1979), *Computational Hydraulics: Elements of the Theory of Free Surface Flows*, Pitman, London.

Andreotti, B., Y. Forterre, and O. Pouliquen (2013), *Granular Media: Between Fluid and Solid*, Cambridge Univ. Press, Cambridge, U. K.

Bagnold, R. A. (1954), Experiments on gravity-free dispersion of large solid spheres in a Newtonian fluid under shear, *Proc. R. Soc. London, Ser. A*, *225*, 49–63.

Basco, D. R. (1983), Computation of rapidly varied, unsteady free surface flow, Water Resources Investigation Report 83–4284, U.S. Geol. Surv., Reston, Va.

Benjamin, T. B., and M. J. Lighthill (1954), On cnoidal waves and bores, *Proc. R. Soc. London, Ser. A*, *224*, 448–460.

Bose, S. K., and S. Dey (2007), Curvilinear flow profiles based on Reynolds averaging, *J. Hydraul. Eng.*, *133*(9), 1074–1079.

Bose, S. K., and S. Dey (2009), Reynolds averaged theory of turbulent shear flows over undulating beds and formation of sand waves, *Phys. Rev. E*, *80*(3), 036304-1–036304-9.

Bouchut, F., and M. Westdickenberg (2004), Gravity driven shallow water models for arbitrary topography, *Commun. Math. Sci.*, *2*, 359–389.

Boussinesq, J. (1872), Théorie des ondes et des remous qui se propagent le long d'un canal rectangulaire horizontal, en communiquant au liquide contenu dans ce canal des vitesses sensiblement pareilles de la surface au fond, *J. Math. Pures Appl.*, *17*, 55–108.

Boussinesq, J. (1877), Essai sur la théorie des eaux courantes, Memoires présentés par divers savants à l'Académie des Sciences, Paris [in French], vol. 23, ser. 3, no. 1, supplément 24, pp. 1–680.

Bronshtein, I., and K. Semendiaev (1971), Mathematical handbook for engineers and students. Ed. Mir, Moscow [translated into Spanish].

Carmo, J. S., F. J. Santos, and A. B. Almeida (1993), Numerical solution of the generalized Serre equations with the MacCormack finite difference scheme, *Int. J. Numer. Methods Fluids*, *16*, 725–738.

Castro-Orgaz, O., and W. H. Hager (2009), Curved streamline transitional flow from mild to steep slopes, *J. Hydraul. Res.*, *47*(5), 574–584.

Castro-Orgaz, O., and W. H. Hager (2011), Turbulent near-critical open channel flow: Serre's similarity theory, *J. Hydraul. Eng.*, *137*(5), 497–503.

Castro-Orgaz, O., J. V. Giráldez, and N. Robinson (2012), Second order two-dimensional solution for the drainage of recharge based on Picard's iteration technique: A generalized Dupuit-Forchheimer equation, *Water Resour. Res.*, *48*, W06516, doi:10.1029/2011WR011751.

Castro-Orgaz, O., J. V. Giráldez, and L. Mateos (2013), Second-order shallow flow equation for anisotropic aquifers, *J. Hydrol.*, *501*, 183–185.

Chaudhry, M. H. (2008), *Open-Channel Flow*, 2nd ed., Springer, Berlin.

Chen, K. C., and Y. C. Tai (2008), Volume-weighted mixture theory of granular materials, *Continuum Mech. Thermodyn.*, *19*, 457–474.

Chen, Q. (2006), Fully nonlinear Boussinesq-type equations for waves and currents over porous beds, *J. Eng. Mech.*, *132*, 220–230.

Chen, Q., J. T. Kirby, R. A. Dalrymple, A. B. Kennedy, and C. M. Haller (1999), Boussinesq modeling of a rip current system, *J. Geophys. Res.*, *104*, 20,617–20,637, doi:10.1029/1999JC900154.

Chen, Q., J. T. Kirby, R. A. Dalrymple, F. Shi, and E. B. Thornton (2003), Boussinesq modeling of longshore currents, *J. Geophys. Res.*, *108*(C11), 3362, doi:10.1029/2002JC001308.

Chen, Y., and P. L. F. Liu (1995), Modified Boussinesq equations and associated parabolic models for water wave propagation, *J. Fluid Mech.*, *288*, 351–381.
Chiou, M.-C., Y. Wang, and K. Hutter (2005), Influence of obstacles on rapid granular flows, *Acta Mech.*, *175*, 105–122.
Denlinger, R. P., and R. M. Iverson (2001), Flow of variably fluidized granular masses across three-dimensional terrain: 2. Numerical predictions and experimental tests, *J. Geophys. Res.*, *106*, 553–566, doi:10.1029/2000JB900330.
Denlinger, R. P., and R. M. Iverson (2004), Granular avalanches across irregular three-dimensional terrain: 1. Theory and Computation, *J. Geophys. Res.*, *109*, F01014, doi:10.1029/2003JF000085.
Denlinger, R. P., and D. R. H. O'Connell (2008), Computing nonhydrostatic shallow-water flow over steep Terrain, *J. Hydraul. Eng.*, *134*(11), 1590–1602.
Dey, S. (2014), *Fluvial Hydrodynamics: Hydrodynamic and Sediment Transport Phenomena*, Springer, Berlin.
Dressler, R. F. (1978), New nonlinear shallow flow equations with curvature, *J. Hydraul. Res.*, *16*(3), 205–222.
Engelund, F., and E. Hansen (1966), *Investigations of Flow in Alluvial Streams*, Bull., vol. 9, Hydraulic Laboratory, Technical Univ. of Denmark, Copenhagen.
Erduran, K. S., S. Ilic, and V. Kutija (2005), Hybrid finite-volume finite-difference scheme for the solution of Boussinesq equations, *Int. J. Numer. Methods Fluids*, *49*, 1213–1232.
Fawer, C. (1937), Etude de quelques ecoulements permanents à filets courbes, thesis, Université de Lausanne, La Concorde, Lausanne, Switzerland.
Gray, J. M. N. T., M. Wieland, and K. Hutter (1999), Gravity driven free surface flow of granular avalanches over complex basal topography, *Proc. R. Soc. London, Ser. A*, *455*, 1841–1874.
Guinot, V. (2003), Riemann solvers and boundary conditions for two dimensional shallow water simulations, *Int. J. Numer. Methods Fluids*, *41*, 1191–1219.
Hager, W. H. (1983), Hydraulics of the plane free overfall, *J. Hydraul. Eng.*, *109*(12), 1683–1697.
Hager, W. H. (2010), Comment on Steady open channel flow with curved streamlines: The Fawer approach revised, *Environ. Fluid Mech.*, *10*(4), 491–494.
Hager, W. H., and K. Hutter (1984a), Approximate treatment of plane channel flow, *Acta Mech.*, *51*(3–4), 31–48.
Hager, W. H., and K. Hutter (1984b), On pseudo-uniform flow in open channel hydraulics, *Acta Mech.*, *53*(3–4), 183–200.
Hungr, O., and N. R. Morgenstern (1984), Experiments on the flow behavior of granular materials at high velocity in an open channel, *Geotechnical*, *34*(3), 405–413.
Hunt, M. L., R. Zenit, C. S. Campbell, and C. E. Brennen (2002), Revisiting the 1954 suspension experiments of R.A. Bagnold, *J. Fluid Mech.*, *452*, 1–24.
Hutter, K. (1996), Avalanche dynamics: A review, in *Hydrology of Disasters*, edited by V. P. Singh, pp. 313–390, Kluwer Acad., Amsterdam.
Hutter, K. (2005), Geophysical granular and particle-laden flows: Review of the field, *Philos. Trans. R. Soc. London*, *363*, 1497–1505.
Hutter, K., and K. Jőhnk (2004), *Continuum Methods of Physical Modeling: Continuum Mechanics, Dimensional Analysis, Turbulence*, 635 pp., Springer, Berlin.
Hutter, K., and T. Koch (1991), Motion of a granular avalanche in an exponentially curved chute: Experiments and theoretical predictions, *Philos. Trans. R. Soc. London, Ser. A*, *334*, 93–138.
Hutter, K., and I. Luca (2012), Two-layer debris mixture flows on arbitrary terrain with mass exchange at the base and the interface, *Continuum Mech. Thermodyn.*, *24*, 525–558.
Hutter, K., and S. B. Savage (1988), Avalanche dynamics: The motion of a finite mass of gravel down a mountain side, 5th Int. Symp. Landslides Lausanne, 691–697.
Hutter, K., M. Siegel, S. B. Savage, and Y. Nohguchi (1993), Two-dimensional spreading of a granular avalanche down an inclined plane part I. Theory, *Acta Mech.*, *100*, 37–68.
Hutter, K., Y. Wang, and S. P. Pudasaini (2005), The Savage-Hutter avalanche model, how far can it be pushed, *Philos. Trans. R. Soc. London*, *363*, 1507–1528.
Iverson, R. M. (1997), The physics of debris flows, *Rev. Geophys.*, *35*(3), 245–296, doi:10.1029/97RG00426.
Iverson, R. M. (2005), Debris-flow mechanics, in *Debris Flow Hazards and Related Phenomena*, edited by M. Jakob and O. Hungr, pp. 105–134, Springer, Heidelberg, Germany.
Iverson, R. M. (2014), Debris flows: Behaviour and hazard assessment, *Geol. Today*, *30*(1), 15–20.
Iverson, R. M., and R. P. Denlinger (2001), Flow of variably fluidized granular masses across three-dimensional terrain: 1. Coulomb mixture theory, *J. Geophys. Res.*, *106*, 537–552, doi:10.1029/2000JB900329.
Iverson, R. M., and J. W. Vallance (2001), New views of granular mass flows, *Geology*, *29*(2), 115–118.
Iverson, R. M., M. E. Reid, and R. G. LaHusen (1997), Debris flow mobilization from landslides, *Ann. Rev. Earth Planet Sci.*, *25*, 85–138.
Iwasa, Y. (1955), Undular jump and its limiting conditions for existence, Proc. 5th Japan Natl. Congress Applied Mech. II-14, 315–319.
Iwasa, Y. (1956), Analytical considerations on cnoidal and solitary waves, *Trans. Jpn. Soc. Civil Eng.*, *32*, 43–49.
Jain, S. C. (2001), *Open Channel Flow*, John Wiley, New York.
Kennedy, A. B., Q. Chen, J. T. Kirby, and R. A. Dalrymple (2000), Boussinesq modeling of wave transformation, breaking, and run-up. I: 1D, *J. Waterw. Port Coastal Ocean Eng.*, *126*, 39–47.
Khan, A. A., and P. M. Steffler (1996a), Modelling overfalls using vertically averaged and moment equations, *J. Hydraul. Eng.*, *122*(7), 397–402.
Khan, A. A., and P. M. Steffler (1996b), Vertically averaged and moment equations model for flow over curved beds, *J. Hydraul. Eng.*, *122*(1), 3–9.
Kim, D.-H., and P. J. Lynett (2011), Dispersive and nonhydrostatic pressure effects at the front of surge, *J. Hydraul. Eng.*, *137*(7), 754–765.
Kim, D.-H., P. J. Lynett, and S. Socolofsky (2009), A depth-integrated model for weakly dispersive, turbulent, and rotational fluid flows, *Ocean Model.*, *27*(3–4), 198–214.
Kuo, C. Y., Y. C. Tai, F. Bouchut, A. Mangeney, M. Pelanti, R. F. Chen, and K. J. Chang (2009), Simulation of Tsaoling landslide, Taiwan, based on Saint Venant equations over general topography, *Eng. Geol.*, *104*, 181–189.
Kuo, C. Y., C. C. Chen, J. J. Dong, Y. C. Tai, K. J. Chang, and A. Y. Siau (2010), Simulation of Shiaolin landslide and focal validation with near-surface magnetic measurements, in *Cross-Strait Workshop on Engineering Mechanics*, Taipei/Tainan, Taiwan.
Kuo, C. Y., Y. C. Tai, C. C. Chen, K. J. Chang, A. Y. Siau, J. J. Dong, R. H. Han, T. Shimamoto, and C. T. Lee (2011), The landslide stage of the Hsiaolin catastrophe: Simulation and validation, *J. Geophys. Res.*, *116*, F04007, doi:10.1029/2010JF001921.
LeVeque, R. J. (2002), *Finite Volume Methods for Hyperbolic Problems*, Cambridge Univ. Press, Cambridge, U. K.
Liggett, J. A. (1994), *Fluid Mechanics*, McGraw-Hill, New York.
Luca, I., K. Hutter, Y. C. Tai, and C. Y. Kuo (2009a), A hierarchy of avalanche models on arbitrary topography, *Acta Mech.*, *205*, 121–149.
Luca, I., Y. C. Tai, and C. Y. Kuo (2009b), Non-Cartesian topography based avalanche equations and approximations of gravity driven flows of ideal and viscous fluids, *Math. Models Methods Appl. Sci.*, *19*(1), 127–171.

Luca, I., K. Hutter, C. Y. Kuo, and Y. C. Tai (2009c), Two layer models for shallow avalanche flows over arbitrary variable topography, *Int. J. Adv. Eng. Appl. Math.*, *1*, 99–121.
Luca, I., C. Y. Kuo, K. Hutter, and Y. C. Tai (2012), Modeling shallow over-saturated mixtures on arbitrary rigid topography, *J. Mech.*, *28*, 523–541.
Lynett, P. J. (2006), Wave breaking effects in depth-integrated models, *Coastal Eng.*, *53*(4), 325–333.
Lynett, P., T. R. Wu, and P. L.-F. Liu (2002), Modeling wave runup with depth-integrated equations, *Coastal Eng.*, *46*(2), 89–107.
Madsen, P. A., and H. A. Schäffer (1998), Higher-order Boussinesq-type equations for surface gravity waves: Derivation and analysis, *Philos. Trans. R. Soc. London, Ser. A*, *356*, 3123–3184.
Madsen, P. A., O. R. Sorensen, and H. A. Schaffer (1997), Surf zone dynamics simulated by a Boussinesq type model. I. Model description and cross-shore motion of regular waves, *Coastal. Eng.*, *32*(4), 255–287.
Mandrup-Andersen, V. (1975), Transition from subcritical to supercritical flow, *J. Hydraul. Res.*, *13*(3), 227–238.
Mandrup-Andersen, V. (1978), Undular hydraulic jump, J. Hydraulics Div. ASCE 104(HY8), 1185-1188; Discussion: 105(HY9), 1208-1211.
Mangeney-Castelnau, A., J.-P. Vilotte, M. O. Bristeau, B. Perthame, F. Bouchut, C. Simeoni, and S. Yerneni (2003), Numerical modeling of avalanches based on Saint Venant equations using a kinetic scheme, *J. Geophys. Res.*, *108*(B11), 2527, doi:10.1029/2002JB002024.
Marchi, E. (1963), Contributo allo studio del risalto ondulato, *G. Genio Civ.*, *101*(9), 466–476.
Marchi, E. (1992), The nappe profile of a free overfall, *Rend. Lincei Mat. Appl. Ser. 9*, *3*(2), 131–140.
Marchi, E. (1993), On the free overfall, *J. Hydraul. Res.*, *31*(6), 777–790.
Matthew, G. D. (1963), On the influence of curvature, surface tension and viscosity on flow over round-crested weirs, *Proc. ICE*, *25*, 511–524.
Matthew, G. D. (1991), Higher order one-dimensional equations of potential flow in open channels, *Proc. ICE*, *91*(3), 187–201.
McDougall, S., and O. Hungr (2003), Objectivities for the development of an integrated three dimensional continuum model for the analysis of landslide runout, in *Debris Hazards Mitigation: Mechanics, Prediction and Assessment*, *Proc. Third Int. Conf.*, edited by D. Rickenmann and C. L. Chen, Mil Press, Rotterdam, Netherlands.
McDougall, S., and O. Hungr (2004), A model for the analysis of rapid landslide motion across three-dimensional terrain, *Can. Geotech. J.*, *42*(5), 1084–1097.
McDougall, S., and O. Hungr (2005), Dynamic modelling of entrainment in rapid landslides, *Can. Geotech. J.*, *41*(6), 1437–1448.
Mei, C. C. (1983), *The Applied Dynamics of Ocean Surface Waves*, John Wiley, New York.
Mignot, E., and R. Cienfuegos (2008), On the application of a Boussinesq model to river flows including shocks, *Coastal Eng.*, *56*(1), 23–31.
Mohapatra, P. K., and M. H. Chaudhry (2004), Numerical solution of Boussinesq equations to simulate dam-break flows, *J. Hydraul. Eng.*, *130*(2), 156–159.
Molls, T., and M. H. Chaudhry (1995), Depth averaged open channel flow model, *J. Hydraul. Eng.*, *121*(6), 453–465.
Montes, J. S. (1986), A study of the undular jump profile, 9th Australasian Fluid Mech. Conf. Auckland, 148–151.
Montes, J. S. (1998), *Hydraulics of Open Channel Flow*, ASCE Press, Reston, Va.
Musumeci, R. E., I. A. Svendsen, and J. Veeramony (2005), The flow in the surf zone: A fully nonlinear Boussinesq-type of approach, *Coastal Eng.*, *52*(7), 565–598.
Naheer, E. (1978), Laboratory experiments with solitary wave, *J. Waterw. Port Coastal Ocean Eng.*, *104*(4), 421–436.
Nwogu, O. (1993), Alternative form of Boussinesq equations for nearshore wave propagation, *J. Waterw. Port Coastal Ocean Eng.*, *119*(6), 618–638.
Pailha, M., and O. Pouliquen (2009), A two-phase flow description of the initiation of underwater granular avalanches, *J. Fluid Mech.*, *636*, 295–319.
Pelanti, M., F. Bouchut, and A. Mangeney (2008), A Roe-type scheme for two-phase shallow granular flows over variable topography, *Math. Modell. Numer. Anal.*, *42*, 851–885.
Peregrine, D. H. (1967), Long waves on a beach, *J. Fluid Mech.*, *27*(5), 815–827.
Pitman, E. B., and L. Le (2005), A two-fluid model for avalanche and debris flows, *Philos. Trans. R. Soc. London*, *A363*, 1573–1602.
Press, W. H., S. A. Teukolsky, W. T. Vetterling, and B. P. Flannery (2007), *Numerical Recipes: The Art of Scientific Computing*, 3rd ed., Cambridge Univ. Press, Cambridge, U. K.
Pudasaini, S. P. (2011), A general two-phase debris flow model, *J. Geophys. Res.*, *117*, F03010, doi:10.1029/2011JF002186.
Pudasaini, S. P., and K. Hutter (2003), Rapid shear flows of dry granular masses down curved and twisted channels, *J. Fluid Mech.*, *495*, 193–208.
Pudasaini, S. P., and K. Hutter (2007), *Avalanche Dynamics*, Springer, Berlin.
Pudasaini, S. P., K. Hutter, and W. Eckart (2003), Gravity-driven rapid shear flows of dry granular masses in topographies with orthogonal and non-orthogonal metrics, in *Dynamic Response of Granular and Porous Materials Under Large and Catastrophic Deformation*, *Lect. Notes Appl. Comput. Mech.*, vol. 11, edited by K. Hutter and N. Kirchner, pp. 43–82, Springer, Berlin.
Pudasaini, S. P., Y. Wang, and K. Hutter (2005a), Dynamics of avalanches along general mountain slopes, *Ann. Glaciol.*, *38*, 257–262.
Pudasaini, S. P., Y. Wang, and K. Hutter (2005b), Modelling two-phase debris flows down general channels and their numerical simulation, *Nat. Hazards Earth Syst. Sci.*, *5*, 799–819.
Pudasaini, S. P., Y. Wang, L.-T. Sheng, S.-S. Hsiau, K. Hutter, and R. Katzenbach (2008), Avalanching granular flows down curved and twisted channels: Theoretical and experimental results, *Phys. Fluids*, *20*, 073302, 1–11.
Rodi, W. (1980), *Turbulence Models and Their Application in Hydraulics: A State of the Art Review*, IAHR, Dordrecht, Netherlands.
Sander, J., and W. H. Hager (1991), Solitäre Wellen, *Österr. Wasserwirtsch.*, *43*(7/8), 185–190.
Sander, J., and K. Hutter (1991), On the development of the theory of the solitary wave: A historical essay, *Acta Mech.*, *86*(1–4), 111–152.
Sander, J., and K. Hutter (1992), Evolution of weakly non-linear shallow water waves generated by a moving boundary, *Acta Mech.*, *91*(3–4), 119–155.
Savage, S. B., and K. Hutter (1989), The motion of a finite mass of granular material down a rough incline, *J. Fluid Mech.*, *199*, 177–215.
Savage, S. B., and K. Hutter (1991), The dynamics of avalanches of granular materials from initiation to runout, Part I. Analysis, *Acta Mech.*, *86*(1–4), 201–223.
Savage, S. B., and R. M. Iverson (2003), Surge dynamics coupled to pore pressure evolution in debris flows, paper presented at 3rd International Conference Debris-Flow Hazards Mitigation, Davos, Switzerland, 503–514.
Serre, F. (1953), Contribution à l'étude des écoulements permanents et variables dans les canaux (Contribution to the study of steady and unsteady channel flows), *Houille Blanche*, *8*(12), 830–887.
Sivakumaran, N. S., and R. F. Dressler (1989), Unsteady density-current equations for highly curved terrain, *J. Atmos. Sci.*, *46*, 3192–3201.
Sivakumaran, N. S., T. Tingsanchali, and R. J. Hosking (1983), Steady shallow flow over curved beds, *J. Fluid Mech.*, *128*, 469–487.
Soares-Frazão, S., and V. Guinot (2008), A second-order semi-implicit hybrid scheme for one-dimensional Boussinesq-type waves in rectangular channels, *Int. J. Numer. Methods Fluids*, *58*(3), 237–261.

Soares-Frazão, S., and Y. Zech (2002), Undular bores and secondary waves: Experiments and hybrid finite-volume modelling, *J. Hydraul. Res.*, *40*(1), 33–43.
Stansby, P. K. (2003), Solitary wave run up and overtopping by a semi-implicit finite-volume shallow-water Boussinesq model, *J. Hydraul. Res.*, *41*(6), 639–647.
Stansby, P. K., and J. G. Zhou (1998), Shallow-water flow solver with non-hydrostatic pressure: 2D vertical plane problems, *Int. J. Numer. Methods Fluids*, *28*(3), 541–563.
Steffler, P. M., and Y. C. Jin (1993), Depth-averaged and moment equations for moderately shallow free surface flow, *J. Hydraul. Res.*, *31*(1), 5–17.
Tai, Y. C., C. Y. Kuo, and W. H. Hui (2012), An alternative to a depth-integrated description for granular avalanches over temporally varying topography with small curvature, *Geophys. Astrophys. Fluid Dyn.*, *106*(6), 596–629.
Toro, E. F. (1997), *Riemann Solvers and Numerical Methods for Fluid Dynamics*, Springer, Berlin.
Toro, E. F. (2002), *Shock-Capturing Methods for Free-Surface Shallow Flows*, Wiley, New York.
Vreugdenhil, C. B. (1994), *Numerical Methods for Shallow Water Flow*, Kluwer, Dordrecht, Netherlands.
Wang, Y., K. Hutter, and S. P. Pudasaini (2004), The Savage-Hutter theory: A system of partial differential equations for avalanche flows of snow, debris and mud, *Z. Angew. Math. Mech.*, *84*(8), 507–527.
Wei, G., and J. T. Kirby (1995), Time-dependent numerical code for extended Boussinesq equations, *J. Waterw. Port Coastal Ocean Eng.*, *121*(5), 251–261.
Wei, G., J. T. Kirby, S. T. Grilli, and R. Subramanya (1995), A fully nonlinear Boussinesq model for surface waves 1: Highly nonlinear unsteady waves, *J. Fluid Mech.*, *294*, 71–92.
Wieland, M., J. M. N. T. Gray, and K. Hutter (1999), Channelised free surface flow of cohesionless granular avalanche in a chute with shallow lateral curvature, *J. Fluid Mech.*, *392*, 73–100.
Yen, B. C. (1973), Open-channel flow equations revisited, *J. Eng. Mech. Div.*, *99*(EM5), 979–1009.